2014

The path to triacylglyceride obesity in the sta6 strain of Chlamydomonas reinhardtii

Ursula Goodenough
Washington University in St Louis

Ian Blaby
University of California - Los Angeles

Sean D. Gallaher
University of California - Los Angeles

Carrie Goodson
Washington University in St Louis

Shannon Johnson
Los Alamos National Laboratory

See next page for additional authors

Eukaryotic Cell

The Path to Triacylglyceride Obesity in the *sta6* Strain of Chlamydomonas reinhardtii

Ursula Goodenough, Ian Blaby, David Casero, Sean D. Gallaher, Carrie Goodson, Shannon Johnson, Jae-Hyeok Lee, Sabeeha S. Merchant, Matteo Pellegrini, Robyn Roth, Jannette Rusch, Manmilan Singh, James G. Umen, Taylor L. Weiss and Tuya Wulan

Eukaryotic Cell **2014, 13(5):591. DOI: 10.1128/EC.00013-14. Published Ahead of Print 28 February 2014.**

EC
Journals.ASM.org

The Path to Triacylglyceride Obesity in the *sta6* Strain of *Chlamydomonas reinhardtii*

Ursula Goodenough,[a] Ian Blaby,[b] David Casero,[c,d]* Sean D. Gallaher,[b] Carrie Goodson,[a] Shannon Johnson,[e] Jae-Hyeok Lee,[f] Sabeeha S. Merchant,[b,d] Matteo Pellegrini,[c,d] Robyn Roth,[g] Jannette Rusch,[a] Manmilan Singh,[h] James G. Umen,[i] Taylor L. Weiss,[a] Tuya Wulan[a]

Department of Biology, Washington University, St. Louis, Missouri, USA[a]; Department of Chemistry and Biochemistry, University of California, Los Angeles, California, USA[b]; Department of Molecular, Cell, and Developmental Biology, University of California, Los Angeles, California, USA[c]; Institute of Genomics and Proteomics, University of California, Los Angeles, California, USA[d]; Genome Science, Los Alamos National Laboratory, Los Alamos, New Mexico, USA[e]; Department of Botany, University of British Columbia, Vancouver, BC, Canada[f]; Department of Cell Biology, Washington University School of Medicine, St. Louis, Missouri, USA[g]; Department of Chemistry, Washington University, St. Louis, Missouri, USA[h]; Danforth Plant Science Center, St. Louis, Missouri, USA[i]

When the *sta6* (starch-null) strain of the green microalga *Chlamydomonas reinhardtii* is nitrogen starved in acetate and then "boosted" after 2 days with additional acetate, the cells become "obese" after 8 days, with triacylglyceride (TAG)-filled lipid bodies filling their cytoplasm and chloroplasts. To assess the transcriptional correlates of this response, the *sta6* strain and the starch-forming *cw15* strain were subjected to RNA-Seq analysis during the 2 days prior and 2 days after the boost, and the data were compared with published reports using other strains and growth conditions. During the 2 h after the boost, ~425 genes are upregulated ≥2-fold and ~875 genes are downregulated ≥2-fold in each strain. Expression of a small subset of "sensitive" genes, encoding enzymes involved in the glyoxylate and Calvin-Benson cycles, gluconeogenesis, and the pentose phosphate pathway, is responsive to culture conditions and genetic background as well as to boosting. Four genes—encoding a diacylglycerol acyltransferase (*DGTT2*), a glycerol-3-P dehydrogenase (*GPD3*), and two candidate lipases (Cre03.g155250 and Cre17.g735600)—are selectively upregulated in the *sta6* strain. Although the bulk rate of acetate depletion from the medium is not boost enhanced, three candidate acetate permease-encoding genes in the *GPR1/FUN34/YaaH* superfamily are boost upregulated, and 13 of the "sensitive" genes are strongly responsive to the cell's acetate status. A cohort of 64 autophagy-related genes is downregulated by the boost. Our results indicate that the boost serves both to avert an autophagy program and to prolong the operation of key pathways that shuttle carbon from acetate into storage lipid, the combined outcome being enhanced TAG accumulation, notably in the *sta6* strain.

Eukaryotic microalgae accumulate storage products—polysaccharides [starch and (chryso)laminarin] and lipids (triacylglycerides [TAG])—when subjected to growth-arresting conditions, such as transfer to nitrogen-free medium (1, 2). When conditions improve, the products are broken down and utilized as sources of carbon backbones, ATP, and reductant. Since TAG represents a potential feedstock for liquid transportation fuel (2–5), much recent research has explored the molecular and cellular parameters associated with TAG biosynthesis.

The green microalga *Chlamydomonas reinhardtii* has been the subject of many of these studies, since it has a rich history of genetic and biochemical analysis (6), a well-annotated genome (7), powerful molecular-genetic tools (6), and a strong starch/TAG response to N deprivation in wild-type strains (8–13). Of particular interest has been the mutant *sta6* strain, which contains a deletion of the gene encoding an ADP-glucose pyrophosphorylase subunit (14, 15) and hence is incapable of starch formation. In most studies, the *sta6* strain produces more TAG than starch-forming strains, such as the *cw15* strain (10, 14, 16–18, 21, 23–25, 48, 72), apparently in large part because it assembles TAG-filled lipid bodies (LBs) in both the chloroplast and the cytoplasm, whereas starch-forming strains produce only cytoplasmic LBs (18). When provided with a "boost" of additional acetate, moreover, the *sta6* strain proceeds to become obese, such that it floats when centrifuged (18). The boost also enhances LB formation in the *cw15* strain, but the cells fail to achieve obesity and do not float (18).

Here we report studies on gene expression patterns during the path to obesity. The Merchant/Pellegrini and Los Alamos laboratories recently generated and analyzed RNA-Seq transcriptomes of the *cw15* and *sta6* mutants and several complemented *sta6* strains during 2 days of N starvation (0⟶48 h NF) (14). In collaboration with these groups, the Goodenough lab generated a second pair of transcriptomes using the *cw15* and *sta6* strains, tracing 0⟶48 h NF gene expression patterns under a different set of culture conditions and taking the time course to 96 h NF, with an intervening acetate boost. Analysis of these data was deeply informed by cross-comparisons with the data obtained by Blaby et al. (14). Three additional RNA-Seq studies of wild-type strains (8, 11, 26) were also considered.

By consolidating these data, it has been possible to identify "robust" biochemical pathways, like starch, fatty acid, and TAG

Received 9 January 2014 Accepted 24 February 2014
Published ahead of print 28 February 2014
Address correspondence to Ursula Goodenough, goodenough@wustl.edu.
* Present address: David Casero, Department of Pathology and Laboratory Medicine, University of California, Los Angeles, California, USA.
Supplemental material for this article may be found at http://dx.doi.org/10.1128/EC.00013-14.

doi:10.1128/EC.00013-14

biosynthesis, wherein patterns of expression of the relevant genes are largely concordant regardless of genetic background or culture conditions, thereby calling attention to the few exceptional cases. Also identified are "sensitive" genes, encoding products operating in several pathways that are influenced by ongoing carbon flux; their expression is coordinated but varies within strains and conditions, suggesting that they play a role in monitoring and responding to N depletion in particular biosynthetic/metabolic contexts. We propose that the several enzymes that are differentially expressed in the *sta6* strain, combined with a glucose-6-phosphate (glucose-6-P) "backflow," participate in generating the chloroplast LBs of this starchless strain. We also propose that the acetate boost deters an autophagy pathway that compromises maximal TAG accumulation.

MATERIALS AND METHODS

Strains. The *sta6* strain (CC-4348; Chlamydomonas Center) is flagellaless and cell wall-less and carries an insertional deletion of the *STA6* gene, encoding the small subunit of ADP-glucose pyrophosphorylase (14, 15) essential for starch biosynthesis. Blaby et al. (14) documented that the *sta6* deletion extends into the neighboring *RBO1* gene and that its contiguous orthologue, *RBO2*, is also attenuated in expression. The *cw15* strain, CC-4349, was considered the clonal parent of the *sta6* strain; however, recent genomic analyses (14) indicate that it is not the parent of the *sta6* strain, since it is the opposite mating type and carries distinctive single nucleotide polymorphisms (SNPs). While its origin is unclear, its flagellar and wall phenotypes are morphologically indistinguishable from those of the *sta6* strain.

Culture conditions in analyzed RNA-Seq data sets. The current RNA-Seq study of the *cw15* and *sta6* strains, designated WUSTL (17 samples per strain), employed cultures grown to 4×10^6 cells/ml in phosphate-buffered high-salt medium (HSM) (28) containing 20 mM potassium acetate at 25 $\mu E\ m^{-2}\ s^{-1}$ light intensity. Cells were harvested by centrifugation ($1{,}153 \times g$ for 3 min) and resuspended in acetate-containing HSM (HSM+acetate) lacking ammonium (nitrogen free [NF]). For the acetate boost, an appropriate aliquot of a 1.5 M potassium acetate stock was added to a culture to augment its acetate concentration by an additional 20 mM.

The two *sta6*/*cw15* data sets from the Merchant/Pellegrini laboratories at the University of California Los Angeles (UCLA) (14), designated UCLA1 (8 samples per strain) and UCLA2 (3 samples per strain), were obtained with cultures grown to 4×10^6 cells/ml in Tris-buffered Tris-acetate-phosphate (TAP) medium (29) containing 17 mM acetate at 95 $\mu E\ m^{-2}\ s^{-1}$ light intensity, harvested by centrifugation ($1{,}006 \times g$ for 5 min), and washed once in NF TAP before resuspension in NF TAP. In some cases, data were also assessed from two RNA-Seq studies of wild-type strains. The first (8), designated UCLA-WT (6 samples), reportedly employed strain CC-3269/2137, but the strain has since been ascertained to be CC-4532; cells were grown and N starved as in the other experiments at UCLA. The second (26), from the Snell laboratory at University of Texas Southwestern Medical school and designated UTSW-WT (3 samples per strain), employed strains CC-1690 mt^+ and CC-1691 mt^- grown in phosphate-buffered Sager and Granick medium (6) without acetate at 50 $\mu E\ m^{-2}\ s^{-1}$ light intensity in either unsynchronized or synchronous cultures before transfer. The mt^+ and mt^- asynchronous cultures were pooled during log phase and prior to RNA extraction, as were the mt^+ and mt^- synchronous cultures, to yield the log reads in Table 8; samples from the synchronous culture were then transferred to N-free, acetate-free Sager and Granick medium for 18 h, and the reads are reported as separate mating types in Table 8. Primary data are found in Table S3 of reference 26.

The WUSTL and the UCLA culture conditions differ in the following respects: (i) medium (HSM+acetate versus TAP), (ii) trace elements (Hutner et al. [30] versus Kropat et al. [31]), (iii) light intensity (25 $\mu E\ m^{-2}\ s^{-1}$ versus 95 $\mu E\ m^{-2}\ s^{-1}$), (iv) culture configuration (500 ml in 1-liter Erlenmeyer flasks versus 1 liter in 2.8-liter Fernbach flasks); (v) flask rotation speed (125 rpm versus 180 rpm), and (vi) the protocol used for transfer to N-free medium (centrifugation duration and one versus two centrifugation steps). Blaby et al. (14) reported a transient stimulation of gene expression in the UCLA samples in conjunction with the centrifugation steps, whereas this was not observed in the WUSTL samples.

Microscopy. Phase and bright-field light microscopy and quick-freeze deep-etch electron microscopy were performed as previously described (18).

Viability analyses. Two methods of analyzing viability were used.

(i) Plating efficiency. A log-phase culture was resuspended in N-free HSM+acetate; after 2 days, the culture was divided, and half was acetate boosted. At each time point, cells were counted, subjected to serial dilutions in TAP medium, mixed with top agar, overlaid on 1.5% TAP agar plates, and allowed to grow until colonies were visible. Plates with scorable colony numbers (50 to 150) were recorded, and the colony number/number of cells plated (plating efficiency) was calculated. The plating efficiency for log-phase cells was set as 100%, and values for N-starved cells, with or without the boost, were expressed proportionately.

(ii) Evans Blue exclusion. A log-phase culture was resuspended in N-free HSM+acetate; after 2 days, the culture was divided, and half was acetate boosted. At each time point, cells were counted, mixed 1:1 with a 0.1% aqueous solution of Evans blue, and scored by light microscopy as viable if dye was excluded. Percent viability was calculated as (viable cell count/original cell count) $\times$ 100.

Acetate uptake. The acetate uptake experiment was performed 3 times with equivalent results; data from one experiment are shown. Vegetative *sta6* cells were grown to 4×10^6 cells/ml in HSM+acetate, pelleted, and resuspended at the same density in N-free HSM+acetate. At the time points indicated in Fig. 4, 7-ml samples were centrifuged at $10{,}000 \times g$ for 5 min; the supernatant was collected by aspiration, passed through a 0.22-μm filter, snap-frozen in liquid N_2, and stored at -20°C until analysis. The filtered medium samples were diluted 50% (vol/vol) with D_2O containing a known amount of alanine, which served as an internal standard. Proton nuclear magnetic resonance (NMR) for these samples were collected on a 14.09-T NMR spectrometer (600 MHz ^{1}H resonance) using a water suppression pulse sequence to suppress the ^{1}H peak due to water in the medium. Each spectrum was collected for 4 scans with a recycle delay of 10 s. The CH_3 protons of alanine are visible at 1.5 ppm, and the CH_3 protons of acetate are visible at 1.9 ppm. The integrated proton peak intensities are directly proportional to the molar ratios of those protons. Hence, the acetate concentrations in the medium samples were determined by comparing the peak integrals of the CH_3 protons of acetate to those of the CH_3 protons of alanine of known concentration.

RNA-Seq analysis. For RNA extraction, cell density was determined with a hemacytometer at each time point. Twenty milliliters of culture was transferred at the time points indicated in Table 1 (maximum cell number per reaction = 2×10^8) to a 50-ml Falcon tube and centrifuged at $2{,}000 \times g$ for 5 min at room temperature. The supernatant was immediately decanted, and the pellets were snap-frozen in liquid N_2 and stored at -80°C.

For processing, samples were brought to room temperature, and the pellets were resuspended in 1 ml freshly made lysis buffer (50 mM Tris-HCl [pH 7.5], 200 mM NaCl, 20 mM EDTA [stock adjusted to pH 8.0], 2% sodium dodecyl sulfate). Ten milliliters of TRIzol (Invitrogen) was then added with thorough mixing, and the samples were incubated for 5 min at room temperature, after which the *cw15* samples were centrifuged at $600 \times g$ for 2 min to pellet starch. The TRIzol solution/lysate was mixed with 1/5 volume of chloroform-isoamyl alcohol (24:1) and shaken vigorously for 15 s. The mixture was incubated for 5 min at room temperature before being transferred to a MaXtract HD (Qiagen) tube. The nucleic acid-containing phase was subsequently separated according to the manufacturer's instructions. To extract RNA, samples were processed using the miRNeasy minikit (Qiagen) according to the manufacturer's instructions. To remove contaminating DNA, samples were on-column digested

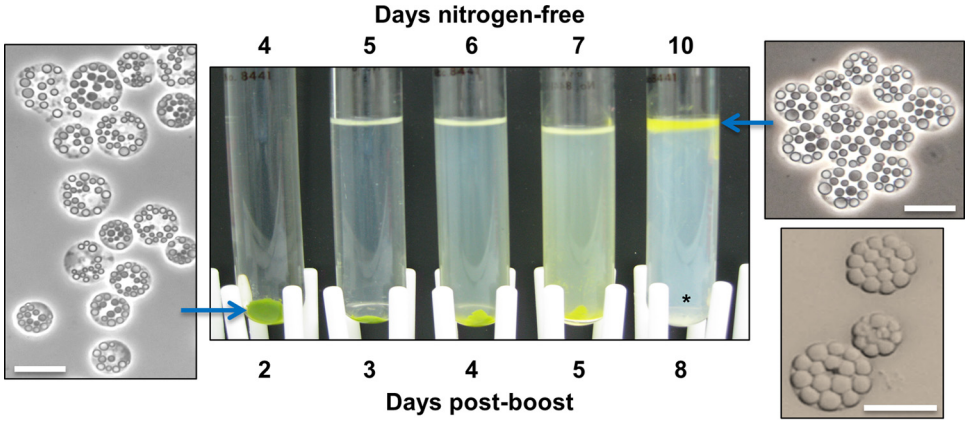

FIG 1 Samples of a *sta6* culture, boosted with 20 mM acetate after 48 h NF and centrifuged at 10,000 × *g* for 5 min at 2, 3, 4, 5, and 8 days postboost. Micrographs show phase and bright-field (lower right) microscopy. Asterisk, cellular debris. Bars, 10 μm.

using the RNase-free DNase set (Qiagen) according to the manufacturer's instructions.

Prior to library preparation, each RNA sample was subjected to quality control evaluation as follows. The concentration and purity of RNA samples were assayed by a NanoDrop spectrophotometer (Thermo Scientific). Each sample was required to have an A_{260}/A_{280} ratio between 2.0 and 2.2 and an A_{260}/A_{230} ratio above 2.0. RNA quality was evaluated by Bioanalyzer (Agilent Technologies) on an Agilent RNA 6000 nanochip following the manufacturer's instructions. RNA integrity was quantified by Agilent 2100 Expert software. Each sample was required to have a RNA integrity number (RIN) above 7.0. The lowest RIN of the WUSTL samples was 7.4; the medians were 8.6 for the *cw15* strain and 8.7 for the *sta6* strain.

cDNA libraries were prepared as described by Boyle et al. (8), and alignments were performed as described by Blaby et al. (14), where reads were aligned to the Aug10.2 gene models (based on the v4 assembly [http://genome.jgi-psf.org/Chlre4/Chlre4.home.html]).

Protein localizations followed the predictions of Blaby et al. (14) and those determined by Predalgo (32) using their web interface (https://giavap-genomes.ibpc.fr/cgi-bin/predalgodb.perl?page=main).

Phylogenetic analyses. The *PDG1* phylogeny (see Fig. S1 in the supplemental material) is a Bayesian consensus tree with bootstrap values from 4,000 iterative samplings using MrBayes (33). *PGD1* homologs were collected from the genome assemblies of V10.2 *C. reinhardtii* (V10.2), *Volvox carteri* (V2), V4 *Ostreococcus tauri* (V4), *Coccomyxa subellipsoidea* C169 (V1), and *Arabidopsis thaliana* (V10). Protein sequences were aligned using MAFFT aligner, followed by manual refinement.

The *GPD* phylogeny (see Fig. S2 in the supplemental material) is a neighbor-joining tree with bootstrap values from 500 replicates. *GPD* homologs were collected from gene models for *C. reinhardtii* (V10.2), *V. carteri* (V1.0), and *Arabidopsis thaliana* (V10). Protein sequences were aligned using the MAFFT aligner, followed by manual refinement. Homology domain information was obtained at the Pfam site (http://pfam.sanger.ac.uk).

The *FBA* phylogeny (see Fig. S3 in the supplemental material) is a Bayesian consensus tree with bootstrap values from 1,000 iterative samplings using MrBayes (33). *FBA* homologs were collected from gene models for *C. reinhardtii* (V10.2), *V. carteri* (V1.0), and *A. thaliana* (V10). Protein sequences were aligned using the MAFFT aligner, followed by manual refinement. The *FBA4* gene is truncated (apparently not due to a gene model error), deleting 100 amino acids at the C terminus, but retains homology to a full-length *V. carteri* member, forming a divergent clade. The topology of the tree was modified to generate coherent family groupings.

The GFY (GPR1/FUN30/YaaH family) phylogenies (see Fig. S5A, C, and D in the supplemental material) were constructed as follows. Multiple sequence alignments were performed using MUSCLE (34) in MEGA 5.2.2 (35). The unrooted neighbor-joining tree for chlorophycean pfam01184 proteins (see Fig. S5D) was generated in MEGA using 500 bootstrap replicates with the model JTT+G (1.4) and pairwise removal of gaps. The unrooted maximum likelihood tree (see Fig. S5C) was generated using PhyML (36) with the model LG+G (1.2) selected using ProtTest (37). Branch scores for the ML tree are derived from an approximate likelihood ratio test. Sequences for phylogenies were obtained as follows. *C. reinhardtii* sequences are from Phytozome gene models as listed. *V. carteri* gene models were based on Phytozome model numbers but manually curated and improved; the protein sequences of the improved *V. carteri* models are found in Data Set S5 in the supplemental material. The remaining sequences were obtained from the Phytozome, JGI UniProt, or NCBI database with the following accession numbers. Phytozome protein IDs are as follows: *Coccomyxa subellipsoidea* C-169, 44355 and 65361; *Ostreococcus lucimarinus*, gwEuk.3.605.1; *Physcomitrella patens*, Pp1s32_336V6.1, Pp1s40_45V6.1, and Pp1_s44_75V6.1. The JGI protein ID for *Emiliania huxleyi* is 240134. UniProt protein IDs were as follows: *Vibrio vulnificus*, Q8DF09; *Escherichia coli*, Q8FLC8; *Leishmania major*, Q9N686; *Methanosarcina acetivorans*, Q8TUG4; *Pasteurella multocida*, Q9CKZ8; *Yarrowia lipolytica*, Q96VC8; *Saccharomyces cerevisiae*, P32907; and *Schizosaccharomyces pombe*, P25613. NCBI protein IDs were as follows: *Wickerhamomyces ciferrii*, GI:406605912; *Ustilago hordei*, GI:388852517.

The GFY similarity network (see Fig. S5B in the supplemental material) was generated according to Atkinson et al. (38) and Blaby-Haas and Merchant (39). Briefly, protein sequences used to generate the network were obtained from the Uniprot90 database (40) using the *GPR1/FUN34/YaaH* domain of Cre17.g702900 (genome version 5.3) as a search query. Any duplicate sequences in the retrieved data were removed, as were sequences resulting from metagenome projects due to unknown eukaryote/prokaryote origin. The resulting 355 protein sequences are found in Data Set S6 in the supplemental material. The network was constructed using a local all-against-all BLASTP (v2.2.28+) search with an E value of $1e^{-29}$. Visualization of the BLASTP output was performed with Cytoscape v2.8.2 (41) using the BLAST2similarityGraph plugin (42).

Gene data accession number. Raw and processed sequence files are available at the National Center for Biotechnology Information Gene Expression Omnibus (accession number GSE55253).

RESULTS

Acquisition of obesity by the *sta6* strain. Figure 1 shows *sta6* cultures that were acetate boosted 2 days after N starvation (48 h

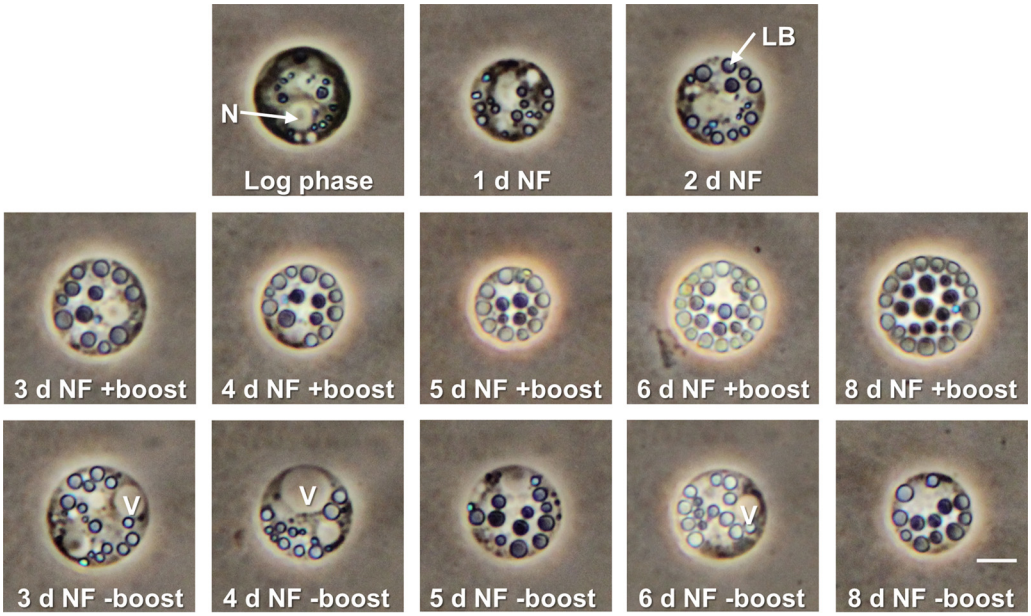

FIG 2 Living *sta6* cells after 1 to 8 days of N starvation with (+) or without (−) acetate boost (phase microscopy). N, nucleus; V, vacuole; LB, lipid body; refractile blue bodies, eyespots. Bar, 5 μm.

NF) and centrifuged (10,000 × *g* for 5 min) 2, 3, 4, 5, and 8 days after the boost. The insets show cells at 2 and 8 days postboost.

Three features are evident. (i) As documented by Goodson et al. (18), the LBs greatly increase in size. (ii) The cells progressively degrade their chlorophyll and become bright yellow, perhaps reflecting the increase in carotenoid content reported for N-starved *C. reinhardtii* (9). (iii) The cells become sufficiently TAG filled that they float, even when centrifuged, the hallmark feature of obesity. Subsequently, the boosted cells die, turn white, and lyse; the released LBs float along with the cells, while the white cellular debris pellets (Fig. 1, asterisk).

Viability of boosted versus nonboosted cells. Figure 2 compares living boosted and nonboosted *sta6* cells using phase microscopy. As previously noted (18), the nonboosted cells display large vacuoles by 3 days in N-free medium, which we interpreted as an indication of morbidity. However, as ascertained by two different assays (see Table S1 in the supplemental material), viability is not compromised until 6 days in N-free medium, after which it slowly declines. Boosted cells display similar viability profiles (see Table S1), but they do not develop large vacuoles and contain more abundant LBs.

Quick-freeze deep-etch EM images of the vacuoles in 96-h NF nonboosted cells are shown in Fig. 3. Contents include profiles of membrane whorls ("myelin figures"), a hallmark of autophagy. No such autophagosomes are encountered in boosted cells. These observations indicate that the boost somehow averts the initiation of an autophagocytic response at 48 h NF, a response that is accompanied by diminished TAG accumulation.

Rates of acetate uptake. An obvious explanation for the boost's ability to enhance TAG content is that after 0→48 h NF, acetate levels in the medium are exhausted and restored by the boost. Alternatively, the boost might enhance the rate of acetate uptake. Either scenario would provide the cells with more substrate for TAG synthesis.

To test these possibilities, NMR was used to determine acetate levels in the culture medium. As previously reported (25), log-phase *sta6* cells take up acetate very rapidly, such that it is exhausted within 48 h of growth, whereas nongrowing N-starved cells utilize it much more slowly. Our results (Fig. 4) confirm these observations: more than half the medium acetate remains after 0→48 h NF, with the mean rate of depletion (193 μmol/h) being similar to the rate observed by Blaby et al. (14) (166 μmol/h). The rate of depletion following the acetate boost (157 μmol/h) is, if anything, lower than before the boost, and samples taken at short intervals following the boost (Fig. 4, inset) show no spike in acetate depletion rates with acetate addition. Hence, neither hypothesis is supported, although a small transient influx is not likely to be detectable by these measurements.

Evidence for a transient acetate influx has instead come from RNA-Seq analysis of boosted *cw15* cells. As documented in Data Set S1B in the supplemental material and summarized in Table 1, an increase in expression of 229 flagellum-related genes is observed within the first 2 h after boost. It has been known for some time that when the pH of the medium is dropped to pH 4.5 with 0.5 N acetic acid for 1 min and then neutralized, *C. reinhardtii* cells first deflagellate and then upregulate expression of their flagellum-related genes and construct new flagella; a recent RNA-Seq profile of these genes (43) strongly overlaps the genes listed in Data Set S1B. Although the *cw15* and *sta6* strains are flagella-less, Cheshire et al. (44) reported that such gene upregulation also occurs in "bald" strains. Deflagellation is induced by several organic acids but not by inorganic acids (45), indicating that entry of organic acids, and not external pH, is the causative event. Even at near-neutral pH, increasing the concentration of exogenous acetate stimulates the deflagellation response (45).

Intriguingly, only 5 flagellum-related genes are upregulated with the boost in the *sta6* strain (Table 1; also, see Data Set S3B in the supplemental material). Acetate (pK_a = 4.76) is known to cross cell membranes in its protonated state and then release the proton into the cytoplasm (46, 47). Therefore, either the cyto-

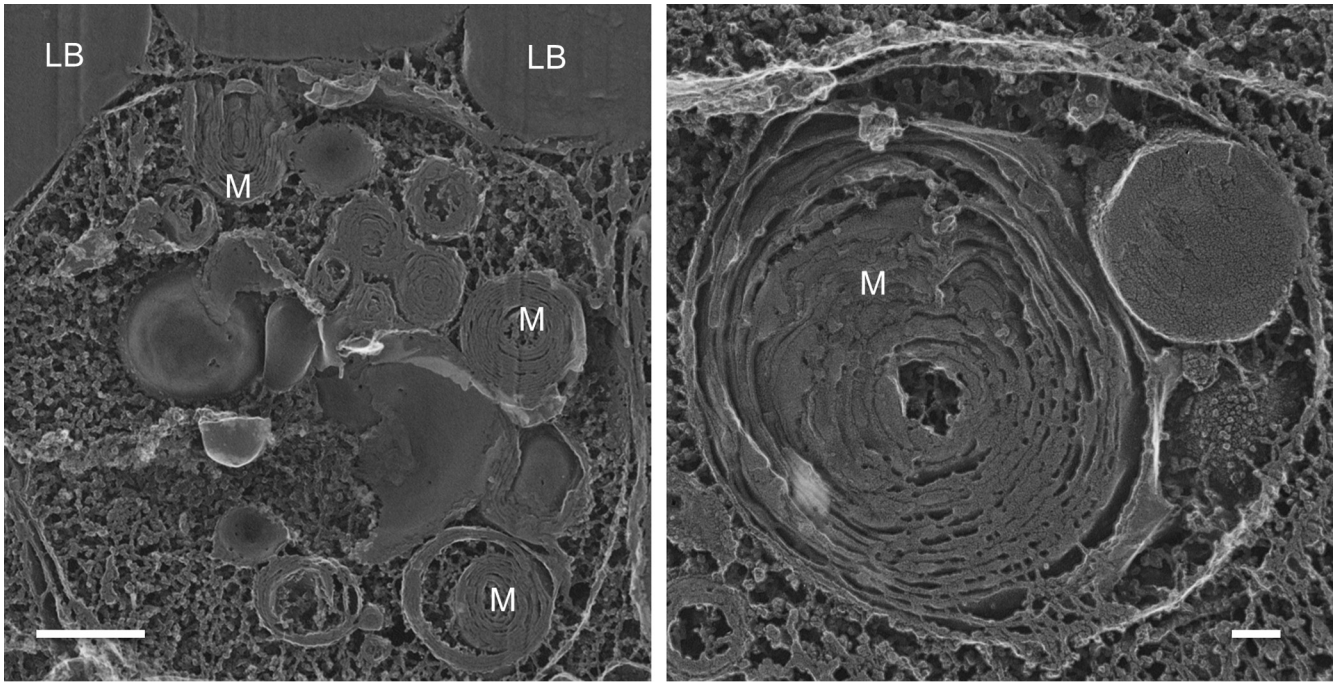

FIG 3 Autophagosomes in 96 h NF nonboosted *sta6* cells. M, myelin figures; LB, cytoplasmic lipid bodies. Bars, 500 nm (left) and 100 nm (right).

plasm of *sta6* cells is at a higher resting pH and/or better buffered than that of *cw15* cells, or the *sta6* strain is for some reason not responsive to some feature of the deflagellation/reflagellation signal, hypotheses we plan to test. Meanwhile, the boost-induced changes in expression of nonflagellar genes, described below, are apparently elicited by stimuli that can act independently of the pathway that elicits the flagellar-gene response, since the nonflagellar responses occur equivalently in both the *cw15* and the *sta6* strains (Table 1).

RNA-Seq experiments: general considerations. Another way that the boost might enhance TAG levels is by influencing gene expression such that, for example, enzymes involved in TAG bio-

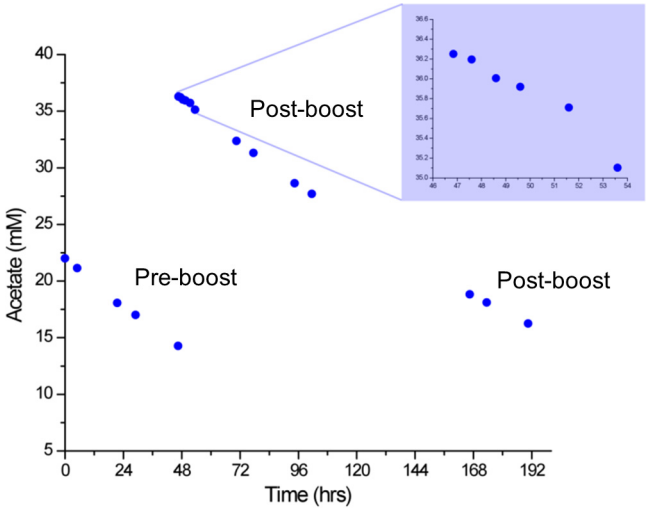

FIG 4 Medium acetate concentrations in an N-starved *sta6* culture preboost and postboost.

TABLE 1 Summary of genes increasing or decreasing expression ≥2-fold relative to 48-h NF levels in response to the acetate boost

Time post-boost	Gene category	Gene entries	Total unique genes responding
cw15 ≥ 2x increase			
0 h	non-flagellar	70	
	flagellar	1	
0.5 h	non-flagellar	331	
	flagellar	185	
2 h	non-flagellar	116	
	flagellar	43	
total	non-flagellar	517	428
	flagellar	229	186
cw15 ≥ 2x decrease			
0 h	all	100	
0.5 h	all	745	
2 h	all	194	
total	all	1039	870
sta6 ≥ 2x increase			
0 h	non-flagellar	186	
	flagellar	0	
0.5 h	non-flagellar	283	
	flagellar	5	
2 h	non-flagellar	193	
	flagellar	3	
total	non-flagellar	662	429
	flagellar	8	7
sta6 ≥ 2x decrease			
0 h	all	95	
0.5 h	all	697	
2 h	all	399	
total	all	1191	875

synthesis and/or polar-lipid recycling are more abundant. To test this thesis, RNA was sampled from *cw15* and *sta6* cultures at nine intervals during 0→48 h NF and at eight intervals during the 2 days following the acetate boost at 48 h NF and subjected to RNA-Seq analysis.

We first identified genes whose expression levels increased or decreased ≥2-fold within the 2 h following acetate boost compared with levels at 48 h NF, where in most cases the boost effect subsided several hours later. Data Sets S1 to S4 in the supplemental material provide complete lists of these genes and their RPKM (reads per kilobase of exon model per million mapped reads) values, where, notably, some half of the genes are not annotated, so we may well be missing some important or even key participants. Table 1 summarizes the outcome. Of the estimated 17,301 genes in v.4 of the *C. reinhardtii* genome, 875 nonflagellar genes displayed a ≥2-fold upshift in the *sta6* strain and 870 displayed such an upshift in the *cw15* strain with the acetate boost, while 429 genes displayed a ≥2-fold downshift in the *sta6* strain and 428 displayed a ≥2-fold down-shift in the *cw15* strain. These numbers might suggest that the same gene sets are responsive in both strains, but this is not the case: only 34% of the upregulated genes are shared, and only 43% of the downregulated genes are shared (identified in Data Sets S1 to S4 in the supplemental material, last column).

We then focused on genes that encode participants in biosynthetic and metabolic pathways related to C and N flux and stress-related processes. The genes considered in this report are highlighted in Data Sets S1 to S4 in the supplemental material. We also queried non-boost-responsive genes that participate in the same pathways as boost-responsive genes.

In analyzing these data, designated WUSTL, we ran comparative studies with the RNA-Seq data on 0→48 h NF in the *cw15* and *sta6* strains, designated UCLA1 (8 samples per strain) and, in some cases, UCLA2 (3 samples per strain) (14), derived from cells cultured under different conditions than the WUSTL conditions. On occasion, we also included data from N-starved wild-type cells maintained in the presence (UCLA-WT) (8) or absence (UTSW-WT) (26) of acetate. Details of strains and culture conditions are provided in Materials and Methods.

A comparison of expression patterns revealed that most of genes involved in the assessed metabolic and biosynthetic pathways were expressed concordantly in the WUSTL and UCLA experiments—e.g., "holding steady," "increasing/decreasing," or "rising and then falling"—even though culture conditions and input transcript levels were disparate, establishing these genes' response to N depletion as "robust" to environmental influence. This steady baseline allowed recognition of the few genes whose expression patterns were not concordant between experiments, where in many cases these genes also proved to be responsive to the acetate boost.

Absent from our data are no-boost controls, and such information would be of particular value with respect to the autophagy-related genes described below. In general, however, the thousands of genes in the data set that did not respond to the boost continued to follow their 0→48 h NF trajectory during the ensuing 48→96 h NF interval, most either holding steady or drifting downward. There is every reason to assume, therefore, that this would also be the case for the boost-responsive genes had a boost not been administered.

Genes related to carbon flux with robust expression patterns.

(i) Starch, fatty acid, and TAG biosynthesis. Expression levels for genes involved with starch, fatty acid, and TAG biosynthesis are shown in Tables 2, 3, and 4.

As initially noted by Blaby et al. (14) and confirmed here, the starch-related genes are uniformly upregulated soon after cells are subjected to N depletion (Table 2, yellow), while genes encoding enzymes involved in fatty acid biosynthesis are upregulated only at 24 h NF (Table 3, yellow), patterns that mirror the observed early increase in starch formation and the later increase in TAG (48). Genes encoding TAG-related enzymes show two patterns: some are upregulated early and then decline, while others show a steady increase, with maximal values at 48 h NF that persist to 96 h NF (Table 4, yellow). The strong concordance of these patterns between the WUSTL and UCLA data sets indicates that these are "robust" genetic programs, akin to those governing expression of chloroplast ribosomal proteins (see Table S2 in the supplemental material), persisting despite differences in strains and culture conditions and despite the fact that the *sta6* strain fails to synthesize any starch and produces chloroplast LBs.

Starch-related genes are generally insensitive to boost; the three exceptions are highlighted in orange in Table 2. Most show a transient increase in expression at 24 h NF in the WUSTL-sta6 samples (Table 2, red).

Fatty acid synthesis-related genes are downregulated at 2 h NF and start recovering at 12 h NF, with maximal expression occurring at 24 h NF and continuing to 96 h NF (Table 3). Transcript levels are consistently higher in the *sta6* strain than the *cw15* strain at 48 h NF and, in the WUSTL data, consistently higher in the *cw15* strain by 96 h NF. While transcription of these genes is not enhanced by the boost, it is briefly depressed in several cases, usually in the *sta6* strain (Table 3, purple). Notably, the five genes encoding subunits of the multimeric "prokaryotic" acetyl coenzyme A (acetyl-CoA) carboxylase (ACCase)—*ACX1*, *BCX1*, *BCR1*, *BXP1*, and *BXP2*—are robustly expressed in both strains (Table 3), whereas the gene Cre08.g373050, encoding a monomeric "eukaryotic" ACCase, produces few (0 to 6 RPKMs) transcripts in both strains (Table 3).

DAG-to-TAG conversion is canonically catalyzed by type 1 (DGAT) and type 2 (DGTT) diacylglycerol acyltransferases. Confirming four reports (8, 11, 13, 14), expression of *DGTT1* is strongly upregulated during 0→48 h NF, with further increases during the next 2 days without a boost response (Table 4), establishing this enzyme as a robust player in the TAG biosynthesis response in all tested strains. Confirming the results reported by Blaby et al. (14), expression of *DGTT2* in the *sta6* strain is initially 3- to 6-fold higher than in the *cw15* strain; by 8 h NF, it tapers to the levels seen in the *cw15* strain, but following the boost, levels are 2-fold higher in the *sta6* strain to 96 h NF (Table 4, blue). This distinctive *DGTT2* transcription pattern is the first of four differences between the *sta6* and *cw15* strains that are highlighted in this report. *DGTT4* and *DGAT1* peak early, and their enhanced levels are sustained to 96 h NF in both strains (Table 4). The WUSTL and UCLA data are dissimilar in two respects: (i) *DGTT3* transcripts peak early and then decline in WUSTL, whereas they peak late in UCLA; and (ii) Cre06.g310200 (DGAT3-like) peaks late in the WUSTL *sta6* sample and in the two *cw15* samples, whereas it peaks early in the UCLA *sta6* sample.

TAG synthesis can also be catalyzed by phospholipid diacylglycerol acyltransferase (PDAT), which uses fatty acids from polar lipids to acylate the DAG hydroxyl group. Recent studies variously reported that PDAT makes a 25% contribution (8) or only a mi-

TABLE 2 Expression profiles (RPKM) of genes participating in starch biosynthesis[a]

	log phase	0 h NF	0.5 h NF	2 h NF	4 h NF	8 h NF	12 h NF	24 h NF	48 h NF	boost	0.5 h PB	2 h PB	4 h PB	8 h PB	12 h PB	24 h PB	48 h PB
STARCH BIOSYNTHESIS																	
Cre03.g175400	PGI1	phosphoglucose isomerase															
WUSTL-cw15	196	225	264	437	272	295	296	228	203	216	209	258	258	242	226	234	233
WUSTL-sta6	229	225	329	465	215	223	199	294	185	219	205	326	271	223	225	241	242
UCLA1-cw15		202	553	490	175	130	148	168	188								
UCLA1-sta6		165	238	469	264	186	208	201	172								
Cre13.g598750	GPM1b	phosphoglucomutase															
WUSTL-cw15	127	166	210	144	78	126	149	93	105	126	68	125	132	139	144	131	125
WUSTL-sta6	269	257	326	211	64	95	109	211	141	125	90	206	168	136	144	156	156
UCLA1-cw15		106	344	133	57	60	75	92	95								
UCLA1-sta6		175	219	213	97	65	87	113	84								
Cre03.g181500	STA11	4-α-glucanotransferase															
WUSTL-cw15	55	50	43	52	47	43	47	41	41	40	25	44	42	43	42	44	42
WUSTL-sta6	70	59	49	72	44	34	35	54	37	32	30	55	47	39	38	34	38
UCLA1-cw15		40	50	44	35	31	35	35	35								
UCLA1-sta6		47	37	81	63	32	36	38	33								
Cre03.g188250	STA6	ADP-glucose pyrophosphorylase small subunit															
WUSTL-cw15	170	170	215	251	203	271	304	148	100	148	112	125	147	152	141	115	107
WUSTL-sta6	3	2	2	2	1	1	1	7	5	5	3	2	3	4	4	4	3
UCLA1-cw15		199	503	390	218	124	147	156	136								
UCLA1-sta6		0	1	1	1	1	1	1	1								
Cre17.g721500	STA2	starch synthase granule-bound															
WUSTL-cw15	110	284	544	397	348	469	505	94	13	40	27	46	59	56	32	28	21
WUSTL-sta6	125	247	411	676	336	285	255	539	47	62	48	162	164	110	113	60	75
UCLA1-cw15		146	680	793	698	315	158	96	24								
UCLA1-sta6		123	470	1132	867	479	395	291	93								
Cre16.g665800	SSS4	soluble starch synthase															
WUSTL-cw15	11	13	24	39	39	62	64	35	20	29	31	28	38	39	33	28	25
WUSTL-sta6	20	16	29	42	21	31	37	101	42	42	42	73	65	59	54	46	44
UCLA1-cw15		16	84	75	42	36	37	35	30								
UCLA1-sta6		12	30	69	56	52	59	70	44								
Cre06.g282000	STA3	glycogen-primed starch synthase															
WUSTL-cw15	49	43	75	217	131	158	145	55	35	50	35	32	40	43	36	36	33
WUSTL-sta6	83	63	108	240	111	118	109	211	94	99	64	124	98	80	75	61	72
UCLA1-cw15		52	261	325	131	81	70	52	39								
UCLA1-sta6		38	60	255	169	113	112	111	60								
Cre06.g289850	SBE1	starch branching enzyme															
WUSTL-cw15	7	5	5	20	19	19	22	25	28	26	14	22	24	23	23	25	27
WUSTL-sta6	12	8	4	17	26	17	20	22	26	22	18	26	23	24	22	24	25
UCLA1-cw15		8	8	32	36	31	32	32	31								
UCLA1-sta6		8	4	24	25	25	24	25	23								
Cre06.g270100	SBE2	starch branching enzyme															
WUSTL-cw15	49	38	66	108	71	67	62	46	29	39	25	35	43	43	40	36	34
WUSTL-sta6	27	17	30	47	28	24	26	17	13	10	11	16	16	14	13	13	13
UCLA1-cw15		15	46	50	36	29	28	20	18								
UCLA1-sta6		16	14	48	31	25	23	20	17								
Cre10.g444700	SBE3	starch branching enzyme															
WUSTL-cw15	83	92	179	422	254	339	392	290	244	365	242	267	391	422	397	324	337
WUSTL-sta6	118	99	179	371	153	167	225	396	239	259	205	263	339	296	273	209	223
UCLA1-cw15		121	416	522	288	222	238	299	275								
UCLA1-sta6		79	173	454	315	293	316	269	169								
Cre03.g185250	SSS2	soluble starch synthase II															
WUSTL-cw15	39	118	44	59	94	48	24	14	21	38	53	19	25	33	35	28	34
WUSTL-sta6	75	73	30	2	4	8	8	80	69	93	189	41	20	23	22	23	26
UCLA1-cw15		120	15	28	26	19	20	31	42								
UCLA1-sta6		119	23	1	2	32	25	35	22								
Cre16.g663850	SSS5	soluble starch synthase															
WUSTL-cw15	7	6	9	22	27	30	36	35	25	26	28	35	39	37	30	33	34
WUSTL-sta6	8	9	19	26	31	31	36	28	18	32	24	40	37	33	32	31	29
UCLA1-cw15		5	24	21	19	19	18	19	18								
UCLA1-sta6		5	22	30	37	27	27	22	21								

[a] Green, boost addition; PB, postboost; yellow, time points of maximum transcripts during 0→48 h NF; orange, genes with ≥2-fold increases in expression relative to 48-h NF levels following acetate boost; red, increased gene expression in WUSTL-sta6 at 24 h NF.

TABLE 3 Expression profiles (RPKM) of genes participating in fatty acid biosynthesis[a]

	log phase	0 h NF	0.5 h NF	2 h NF	4 h NF	8 h NF	12 h NF	24 h NF	48 h NF	boost	0.5 h PB	2 h PB	4 h PB	8 h PB	12 h PB	24 h PB	48 h PB
FATTY ACID BIOSYNTHESIS																	
Cre12.g519100	ACX1	α-carboxyltransferase subunit of plastidic multimeric ACCase															
WUSTL-cw15	77	90	114	36	49	71	113	177	178	212	135	142	281	324	305	296	283
WUSTL-sta6	123	71	79	26	40	76	151	262	169	233	209	104	176	231	228	202	188
UCLA1-cw15		53	64	73	124	150	180	259	231								
UCLA1-sta6		57	50	47	101	185	203	187	164								
Cre12.g484000	BCX1	β-carboxyltransferase subunit of plastidic multimeric ACCase															
WUSTL-cw15	67	81	98	36	40	60	89	120	124	144	95	113	227	243	207	196	199
WUSTL-sta6	111	79	75	31	32	51	100	162	99	147	128	75	143	167	159	140	120
UCLA1-cw15		86	57	62	78	94	121	159	146								
UCLA1-sta6		64	48	42	79	123	123	115	104								
Cre08.g359350	BCR1	biotin carboxylase subunit of plastidic multimeric ACCase															
WUSTL-cw15	131	167	168	35	31	56	98	174	203	182	116	131	287	378	360	306	293
WUSTL-sta6	185	183	129	41	28	52	108	321	201	194	159	77	180	236	221	194	172
UCLA1-cw15		208	78	69	131	143	168	257	250								
UCLA1-sta6		156	107	57	88	192	219	224	156								
Cre17.g715250	BXP1	biotin carboxyl carrirer subunit of plastidic multimeric ACCase															
WUSTL-cw15	116	138	137	38	32	49	87	157	175	156	101	124	279	291	267	242	237
WUSTL-sta6	177	159	128	36	24	47	117	254	145	172	157	95	178	224	214	182	165
UCLA1-cw15		171	96	85	123	102	138	234	226								
UCLA1-sta6		130	105	62	90	166	196	200	170								
Cre01.g037850	BXP2	biotin carboxyl carriersubunit of plastidic multimeric ACCase															
WUSTL-cw15	149	180	185	44	30	45	80	145	186	172	78	92	231	328	290	258	236
WUSTL-sta6	218	190	160	36	30	48	119	265	170	187	150	72	180	250	235	192	171
UCLA1-cw15		227	86	64	80	72	95	173	183								
UCLA1-sta6		149	97	40	69	146	171	173	148								
Cre13.g577100	ACP2	acyl-carrier protein															
WUSTL-cw15	1849	1918	1994	596	553	1160	1704	1958	1978	2173	1230	1401	2163	2637	2466	1969	1941
WUSTL-sta6	2123	2179	2009	1104	336	646	1500	3003	2302	2284	1750	1126	1630	1930	1979	1647	1468
UCLA1-cw15		1750	1413	563	844	875	1077	1753	1767								
UCLA1-sta6		1356	1133	686	682	1280	1583	1663	1147								
Cre14.g621650	MCT1	malonyl-CoA:acyl-carrier-protein transacylase															
WUSTL-cw15	57	71	64	29	15	10	12	19	21	25	15	16	39	56	52	41	34
WUSTL-sta6	95	95	81	52	27	11	12	53	23	26	31	12	34	42	40	32	28
UCLA1-cw15		81	52	19	24	17	19	35	34								
UCLA1-sta6		66	54	37	37	38	37	40	26								
Cre22.g765250	KAS1	3-ketoacyl-CoA-synthase															
WUSTL-cw15	178	196	171	36	35	59	100	207	246	222	156	150	323	401	364	312	314
WUSTL-sta6	253	257	204	25	24	55	161	351	263	266	247	92	220	282	268	218	209
UCLA1-cw15		229	99	51	68	87	139	269	311								
UCLA1-sta6		204	156	30	72	185	220	246	204								
Cre07.g335300	KAS2	3-ketoacyl-ACP-synthase															
WUSTL-cw15	27	27	33	12	13	16	23	25	17	27	21	21	43	56	47	41	38
WUSTL-sta6	36	22	20	7	8	12	26	48	18	31	25	19	29	32	32	24	19
UCLA1-cw15		18	11	23	28	23	25	36	34								
UCLA1-sta6		20	6	13	25	36	37	32	21								
Cre04.g216950	KAS3	3-ketoacyl-ACP synthase															
WUSTL-cw15	28	37	20	7	8	9	13	17	14	17	9	11	26	31	27	24	23
WUSTL-sta6	40	32	20	2	4	5	13	17	12	17	12	6	13	16	16	12	10
UCLA1-cw15		44	4	12	18	15	20	33	36								
UCLA1-sta6		36	16	3	11	21	17	14	15								
Cre03.g172000	KAR1	3-ketoacyl-ACP reductase															
WUSTL-cw15	106	106	111	75	29	16	23	42	46	46	32	45	63	81	75	55	54
WUSTL-sta6	130	122	104	50	17	11	23	103	52	48	48	19	48	63	59	41	37
UCLA1-cw15		113	77	66	43	20	33	70	75								
UCLA1-sta6		111	82	44	60	72	60	70	43								
Cre06.g294950	ENR1	enoyl-ACP-reductase															
WUSTL-cw15	273	278	273	179	115	104	136	157	148	159	141	133	223	276	251	191	173
WUSTL-sta6	321	307	260	101	38	61	150	348	199	228	192	86	155	191	169	160	124
UCLA1-cw15		340	208	183	180	102	154	250	255								
UCLA1-sta6		276	202	116	127	158	187	206	126								
Cre08.g373050		eukaryotic ACCase															
WUSTL-cw15	4	3	4	2	2	1	1	2	2	2	0	2	2	1	2	2	2
WUSTL-sta6	3	2	2	2	4	1	1	3	3	3	1	2	2	2	2	2	2
UCLA1-cw15		4	6	5	4	3	4	4	5								
UCLA1-sta6		3	1	2	2	2	2	3	2								

[a] Green, boost addition; PB, postboost; yellow, time points of maximum transcripts during 0→48 h NF; purple, genes ≥2-fold decreases in expression relative to 48-h NF levels following acetate boost.

TABLE 4 Expression profiles (RPKM) of genes participating in TAG biosynthesis[a]

	log phase	0 h NF	0.5 h NF	2 h NF	4 h NF	8 h NF	12 h NF	24 h NF	48 h NF	boost	0.5 h PB	2 h PB	4 h PB	8 h PB	12 h PB	24 h PB	48 h PB
TAG BIOSYNTHESIS																	
Cre01.g045900	**DGAT1**	**DAGAT type 1**															
WUSTL-cw15	3	2	3	17	8	10	11	12	13	14	8	9	12	14	13	12	10
WUSTL-sta6	4	4	8	14	11	12	15	12	9	14	6	10	12	12	10	8	10
UCLA1-cw15		2	14	36	29	17	20	19	18								
UCLA1-sta6		5	6	23	20	18	17	15	13								
UCLA-WT		3		12		15	15	9	21								
Cre12.g557750	**DGTT1**	**DAGAT type 2**															
WUSTL-cw15	0	0	0	6	7	17	23	33	35	40	51	41	51	55	45	42	44
WUSTL-sta6	1	0	1	8	11	23	34	47	42	49	35	44	58	58	59	52	53
UCLA1-cw15		0	2	20	17	28	32	43	47								
UCLA1-sta6		0	0	14	20	34	37	38	41								
UCLA-WT		1		8		17	11	18	25								
Cre02.g121200	**DGTT2**	**DAGAT type 2**															
WUSTL-cw15	25	21	27	26	26	24	30	33	36	41	31	28	32	36	32	32	31
WUSTL-sta6	103	99	163	144	80	35	36	44	65	48	32	54	62	64	63	68	69
UCLA1-cw15		19	26	27	33	34	36	35	37								
UCLA1-sta6		73	112	80	68	49	51	39	45								
UCLA2-cw15			22		22			43									
UCLA2-sta6			165		72			19									
UCLA-WT		22		21		22	25	26	27								
Cre06.g299050	**DGTT3**	**DAGAT Type 2**															
WUSTL-cw15	39	22	50	34	31	33	38	34	29	38	30	34	42	41	39	36	37
WUSTL-sta6	35	19	43	42	36	36	42	39	28	34	27	27	32	34	30	30	28
UCLA1-cw15		12	32	27	31	31	34	39	38								
UCLA1-sta6		18	18	37	46	45	47	41	41								
UCLA-WT		35		33		27	32	41	32								
Cre03.g205050	**DGTT4**	**diacylglycerol acyl transferase**															
WUSTL-cw15	7	2	12	9	5	8	8	4	4	7	4	5	6	7	7	5	5
WUSTL-sta6	5	1	7	10	6	3	3	9	5	3	7	4	4	5	4	3	3
UCLA1-cw15		1	17	10	12	6	7	8	7								
UCLA1-sta6		4	2	5	4	6	5	6	4								
UCLA-WT		5		8		6	8	3	3								
Cre06.g310200	**DGAT3-like**																
WUSTL-cw15	26	21	41	24	38	56	64	78	96	135	114	105	101	94	94	96	109
WUSTL-sta6	49	40	57	51	45	67	80	89	119	206	129	111	103	107	97	115	124
UCLA1-cw15		10	21	26	31	28	19	22	35								
UCLA1-sta6		26	56	88	80	69	67	80	63								
UCLA-WT		19		8		24	32	46	45								
Cre02.g106400	**PDAT1**	**phospholipid diacylglycerol acyltransferase**															
WUSTL-cw15	12	12	9	18	14	17	17	14	15	14	3	8	12	10	10	11	10
WUSTL-sta6	15	11	9	22	16	21	22	18	17	14	4	12	12	13	10	10	11
UCLA1-cw15		6	9	22	17	13	16	15	14								
UCLA1-sta6		9	4	24	20	15	14	12	9								
UCLA-WT		3		9		9	8	10	8								
Cre06.g299800	**FAT**	**long-chain-fatty-acid CoA ligase**															
WUSTL-cw15	3	4	3	2	6	9	10	11	17	20	33	30	19	16	23	22	28
WUSTL-sta6	3	1	1	0	1	3	3	25	32	34	81	41	28	32	32	27	40
UCLA1-cw15		1	1	1	1	7	10	15	22								
UCLA1-sta6		2	0	0	0	1	3	14	19								
UCLA-WT		5		2		9	11	8	9								
Cre01.g037700	**FAD3**	**fatty acid desaturase**															
WUSTL-cw15	26	33	88	85	52	89	99	43	26	38	33	62	68	75	70	62	63
WUSTL-sta6	22	16	60	60	25	24	24	31	8	10	17	22	26	25	26	16	18
UCLA1-cw15		22	129	117	92	55	46	59	54								
UCLA1-sta6		12	30	60	47	39	36	21	14								
UCLA-WT		57		54		48	37	37	27								
Cre03.g182050	**LCS1**	**putative long-chain acyl-CoA synthetase**															
WUSTL-cw15	71	90	77	81	99	111	124	117	166	186	95	87	107	118	114	128	142
WUSTL-sta6	67	73	54	60	78	102	129	160	232	201	91	84	103	118	119	107	115
UCLA1-cw15		92	45	86	97	117	132	133	150								
UCLA1-sta6		77	56	64	81	102	104	121	112								
Cre13.g566650	**LCS2**	**putative long-chain acyl-CoA synthetase**															
WUSTL-cw15	37	42	46	61	41	68	100	135	132	137	138	116	191	212	185	170	164
WUSTL-sta6	80	62	54	80	58	77	142	204	162	167	158	141	198	212	199	165	159
UCLA1-cw15		43	43	125	108	117	143	170	149								
UCLA1-sta6		41	21	96	102	129	139	134	107								
Cre09.g405500	**MLDP**	**major lipid droplet protein**															
WUSTL-cw15	19	18	12	35	139	256	403	551	500	484	474	511	670	669	639	606	634
WUSTL-sta6	24	18	12	24	130	279	467	494	384	401	393	442	627	588	587	653	536
UCLA1-cw15		12	19	47	129	232	230	234	216								
UCLA1-sta6		23	19	58	259	458	477	426	441								
UCLA-WT		12		31		192	225	168	158								

[a] Green, boost addition; PB, postboost. Yellow, time points of maximum transcripts during 0→48 h NF; orange, genes with ≥2-fold increases in expression relative to 48-h NF levels following acetate boost; purple, genes decreasing expression ≥2-fold relative to 48-h NF levels following acetate boost; blue, genes showing strong differential expression between the *sta6* and *cw15* strains.

nor contribution (27) to TAG synthesis under N-deprivation conditions. Transcription from *PDAT1* peaks early and remains steady in all three strains, with a transient downregulation at the boost (Table 4).

Two other lipid-related genes augmented with the boost in both strains are Cre06.g299800 (long-chain-fatty acid CoA ligase) and *FAD3* (fatty acid desaturase) (Table 4). A putative long-chain acyl-CoA synthetase (*LCS1*) decreases with the boost, while a second (*LCS2*) is not affected (Table 4).

Expression of the *MLDP1* gene increases 28-fold in the *cw15* strain and 21-fold in the *sta6* strain during 0→48 h NF and is sustained at high levels for the next 2 days without a boost response; similar increases are seen in the UCLA and UCLA-WT data (Table 4). The gene product, originally posited to be associated with lipid bodies (major lipid droplet protein) (12), has recently been shown to instead be associated with endoplasmic reticulum (ER) membranes (49), where it possibly participates in the intimate ER/LB associations that are established during cytoplasmic LB formation in N-free medium (18).

(ii) Lipases. In their pioneering RNA-Seq study, Miller et al. (11) identified 130 *C. reinhardtii* genes carrying the GXSXG motif expected of lipases, of which 46 were either upregulated (75%) or downregulated (25%) ≥2-fold in wild-type cells during 0→48 h NF, and they posited that a subset of these might be involved in releasing fatty acids from polar lipids for use in TAG formation in the fashion of the PDAT enzyme. In a subsequent paper (50), the lab reported that one of these genes, designated Cre03.g193500 and now named *PGD1* (plastid galactoglycerolipid degradation), indeed contributes to TAG formation by breaking down pre-existing chloroplast monogalactosyldiacylglycerol (MGDG) into its lyso-lipid form for reacylation as TAG; knockdown of this gene results in reduced TAG accumulation with N starvation.

The WUSTL RNA-Seq data for these 46 candidate lipase genes are shown in Table S3 in the supplemental material; four genes annotated as TAG lipases and not included in the 46-gene set are also listed. Expression is generally equivalent for the *cw15* and *sta6* strains and generally equivalent in the WUSTL and UCLA data sets (data not shown). Except for a spike at 2 h NF for two of the genes (see Table S3, yellow), most display either steady or gradually increasing expression, with some showing small boost responses. The three genes in blue in Table S3 are displayed in Table 5 and given additional attention below.

As anticipated, *PGD1* expression increases strongly throughout the N starvation time course in all strains (Table 5). The PDG1 protein lacks a predicted leader sequence, but since MGDG is restricted to thylakoids, a chloroplast location is considered likely.

Two homologues of *PDG1* were identified (see Fig. S1 in the supplemental material). The first, Cre05.g248200/g5168, carries a high-scoring chloroplast transit sequence and is the only gene in the candidate-lipase cohort that decreases expression in all strains during the time course (Table 5).

The second *PGD1* homologue, Cre03.g155250 (not included in the 46-gene set), is more strongly predicted to be mitochondrion localized (M score, 0.825) than chloroplast localized (C score, 0.444), and a mitochondrial TAG lipase was recently detected in yeast (51); that said, organelle transit sequences can be difficult to differentiate in *C. reinhardtii*, and direct localization experiments are needed. Cre03.g155250 is expressed in all strains at early time points, but transcript levels then plummet in the *cw15* strain and the wild type, whereas they strongly increase in the *sta6* strain, with a 2.7-fold boost (Table 5, blue). The distinctive transcription pattern of Cre03.g155250 is the second of four *sta6*/*cw15* differences that are highlighted in this report.

Another candidate lipase-encoding gene also displays differential expression in the *sta6* strain. Cre17.g735600 (not included in the 46-gene set) encodes a protein with a strongly predicted signal peptide, which usually indicates an ER→secretory destination but in some cases directs proteins to the chloroplast (20, 52). The gene is not expressed in UCLA-WT or in the *cw15* strain, except for a brief spike at the boost, but is robustly expressed by *sta6* in both the WUSTL and UCLA1/UCLA2 experiments (Table 5, blue), with a 2.5-fold increase with the boost (Table 5, orange). Cre17.g735600 is related to three other *C. reinhardtii* genes (data not shown): Cre09.g399400 and Cre14.g615550 yield no transcripts in either strain, while Cre02.g127300 shows a steady increase in both (see Table S3 in the supplemental material). The distinctive transcription pattern of Cre17.g735600 is the third of four *sta6*/*cw15* differences that are highlighted in this report.

Cre02.g127550 (g9712 in the v.5.3 assembly), which lacks a predicted leader sequence, displays strong expression in the *sta6* strain but weak expression in the *cw15* strain, except for a brief spike at the boost, throughout the 96-h time course in the WUSTL experiment (Table 5). However, expression of this gene is anomalous. In the two UCLA experiments, transcripts are either somewhat more abundant in the *cw15* strain than the *sta6* strain (UCLA1) or equivalent (UCLA2); moreover, the gene shows no expression in UCLA-WT (Table 5), whereas it is the most strongly upregulated candidate lipase (5.6-fold) in the wild-type experiment described by Miller et al. (11). This example emphasizes the value of having several data sets when assigning expression patterns to particular strains: such anomalies, and this one is obviously of interest, presumably indicate sensitivity to particular culture conditions rather than a strain-specific trait.

(iii) Fatty acid β-oxidation enzymes. TAG accumulation operates in opposition to TAG breakdown. The fatty acids released from the breakdown of both neutral and polar lipids are processed by the β-oxidation pathway. In their RNA-Seq comparison of wild-type cells at 0 h and 48 h NF, Miller et al. (11) noted >3-fold-decreased transcript levels for two enzymes in this pathway, acyl-CoA oxidase (Cre16.g689050) and 3-oxoacyl-CoA thiolase (Cre17.g723650, *ATO1*), and a 2-fold increase for a third, enoyl-CoA hydratase (Cre03.g190850, *ECH1*). Similar patterns were seen in the present experiments (see Table S4 in the supplemental material): expression levels of the oxidase gene declined slightly and those of the thiolase gene more substantially, while the hydratase levels increased. Interestingly, levels of thiolase and hydratase transcripts increased 3.9-fold and 1.6-fold, respectively, with the acetate boost for the *sta6* strain, with no boost effect for the *cw15* strain, and thiolase gene expression remained stronger in the *sta6* strain to 96 h NF (see Table S4). Therefore, the boost appears to selectively enhance the machinery for fatty acid breakdown in the *sta6* strain, perhaps in part in conjunction with the breakdown and remodeling of thylakoid membranes undertaken by *sta6* at later time points in the N-starvation sequence (18).

(iv) Glycerol-3-P dehydrogenase. Glycerol-3-P serves as the backbone for DAG and TAG biosynthesis and can thus be said to serve as a bridge between carbohydrate and lipid biosynthesis. It also drives a mitochondrial shuttle system engaged in the import of NADH (53). Glycerol-3-P is generated from dihydroxyacetone phosphate (DHAP), a sugar produced during both gluconeogen-

TABLE 5 Expression profiles (RPKM) of genes encoding candidate lipases[a]

	log phase	0 h NF	0.5 h NF	2 h NF	4 h NF	8 h NF	12 h NF	24 h NF	48 h NF	boost	0.5 h PB	2 h PB	4 h PB	8 h PB	12 h PB	24 h PB	48 h PB
CANDIDATE LIPASES																	
Cre03.g193500		PDG1			plastid galactoglycerolipid degradation												
WUSTL-cw15	8	5	10	13	14	29	47	88	75	101	76	83	122	132	120	142	146
WUSTL-sta6	8	4	6	9	15	26	53	99	65	100	62	49	79	101	104	87	83
UCLA1-cw15		6	9	37	40	53	60	92	102								
UCLA1-sta6		8	5	17	39	46	61	62	58								
UCLA2-cw15			10		19			10									
UCLA2-sta6			5		9			72									
UCLA-WT		12		13		17	18	21	13								
Cre05.g248200/g5168				lipase class 3													
WUSTL-cw15	17	13	18	16	14	10	8	9	11	9	10	8	7	7	8	9	9
WUSTL-sta6	17	12	15	14	14	12	11	9	9	12	10	8	7	7	7	7	8
UCLA1-cw15		20	9	8	3	5	6	6	6								
UCLA1-sta6		20	5	9	9	11	8	8	8								
UCLA2-cw15			3		3				2								
UCLA2-sta6			4		3				1								
UCLA-WT		5		4		3	5	3	1								
Cre03.g155250																	
WUSTL-cw15	17	34	12	15	24	11	2	0	0	0	3	2	1	1	1	1	2
WUSTL-sta6	32	13	9	1	2	5	4	15	17	29	45	13	7	8	5	9	14
UCLA1-cw15		84	2	1	1	2	2	1	2								
UCLA1-sta6		109	1	0	1	6	3	10	12								
UCLA2-cw15			11		41				8								
UCLA2-sta6			1		6				8								
UCLA-WT		24		9		7	14	6	5								
Cre17.g735600				TAG lipase													
WUSTL-cw15	1	1	2	3	2	2	2	2	2	2	12	3	2	2	1	1	2
WUSTL-sta6	19	9	28	39	33	26	23	22	21	25	51	50	41	35	35	34	41
UCLA1-cw15		2	6	8	8	9	10	11	9								
UCLA1-sta6		13	24	65	52	44	45	49	47								
UCLA2-cw15			12		14				4								
UCLA2-sta6			22		28				32								
UCLA-WT		0		0		0	0	0	0								
Cre02.g127550/g9712				lipase class 3													
WUSTL-cw15	0	0	0	0	0	1	2	3	8	5	16	5	3	2	1	2	1
WUSTL-sta6	6	3	2	22	41	36	35	74	185	192	94	50	68	92	100	77	52
UCLA1-cw15		0	0	19	52	88	77	28	8								
UCLA1-sta6		0	0	7	10	17	51	58	26								
UCLA2-cw15			3		7				34								
UCLA2-sta6			0		6				42								
UCLA-WT		0		0		0	0	0	0								

[a] Green, boost addition; PB, postboost; orange, genes with ≥2-fold increases in expression relative to 48-h NF levels following acetate boost; blue, genes showing strong differential expression between the *sta6* and *cw15* strains.

esis and the Calvin-Benson cycle, via NADH-dependent glycerol-3-P dehydrogenases (GPDH) (the mitochondrial enzymes are $FADH_2$ dependent). NADH-dependent GPDHs are encoded by five genes in *C. reinhardtii* (Table 6), one of which (*GPD5*) was identified during this study.

Table 6 summarizes their expression patterns. *GPD1* (Cre12.g511150) and *GPD5* (Cre02.g122300/g9595), with no predicted targeting sequences, are expressed constitutively at low levels throughout the time course. *GPD2* (Cre01.g053000) transcripts, predicted to be chloroplast targeted, increase 26-fold in the *cw15* strain and 24-fold in the *sta6* strain during 0→48 h NF; the boost increases transcript levels 2-fold more in the *cw15* strain and 2.3-fold more in the *sta6* strain, and high levels are sustained to 96 h NF. *GPD4* (Cre10.g421700), also predicted to be chloroplast directed, increases expression during 0→48 h NF (4.3-fold for the *cw15* strain and 6.2-fold for the *sta6* strain) and sustains high levels to 96 h NF without responding to the boost, with levels being consistently higher in the *sta6* strain than in the *cw15* strain. Large increases in *GPD2* and *GPD4* transcripts during 0→48 h NF, and the *sta6* bias for *GPD4*, are also seen in the UCLA and UCLA-WT data (Table 6).

Particularly striking is the pattern of *GPD3* (Cre01.g053150), which carries no predicted leader sequence. Its expression level remained very low throughout the 0→48 h NF period in both strains in both experiments but then shot up 30-fold with the boost in the *cw15* strain and 72-fold in the *sta6* strain (Table 6). Moreover, while transcript levels then abated in the *cw15* strain to 39% of their maximum boost levels by 96 h NF, they continued to

TABLE 6 Expression profiles (RPKM) of genes encoding glycerol-3-P dehydrogenase[a]

	log phase	0 h NF	0.5 h NF	2 h NF	4 h NF	8 h NF	12 h NF	24 h NF	48 h NF	boost	0.5 h PB	2 h PB	4 h PB	8 h PB	12 h PB	24 h PB	48 h PB
GPD GENES																	
Cre12.g511150	GPD1	glycerol-3-phosphate dehydrogenase															
WUSTL-cw15	11	15	18	10	10	12	13	9	9	15	12	9	13	15	15	13	12
WUSTL-sta6	9	4	8	4	4	7	8	15	12	19	19	10	10	11	11	10	10
UCLA1-cw15		12	16	11	14	11	11	11	12								
UCLA1-sta6		16	20	10	9	9	10	9	9								
UCLA-WT		19		10		14	12	11	10								
Cre01.g053000	GPD2	glycerol-3-P dehydrogenase															
WUSTL-cw15	12	17	40	35	68	161	273	362	441	397	900	731	763	761	686	744	822
WUSTL-sta6	17	24	30	86	85	192	462	466	578	823	1327	727	833	1064	1119	1074	1069
UCLA1-cw15		6	77	113	219	518	599	729	916								
UCLA1-sta6		15	11	312	478	407	469	609	895								
UCLA-WT		24		50		209	154	188	214								
Cre01.g053150	GPD3	glycerol-3-P dehydrogenase															
WUSTL-cw15	2	2	1	1	4	7	7	6	2	2	59	43	29	30	30	15	23
WUSTL-sta6	2	2	1	2	7	4	2	1	2	12	128	143	200	163	156	247	278
UCLA1-cw15		0	0	0	1	3	5	7	8								
UCLA1-sta6		0	0	1	2	2	2	3	5								
UCLA-WT		9		1		2	1	0	7								
Cre10.g421700	GPD4	glycerol-3-P dehydrogenase															
WUSTL-cw15	14	29	16	43	41	62	79	119	126	93	89	107	133	124	111	116	105
WUSTL-sta6	22	18	27	72	77	126	153	117	111	120	73	133	190	167	156	171	163
UCLA1-cw15		8	18	59	66	99	134	128	127								
UCLA1-sta6		14	8	99	172	228	219	191	177								
UCLA-WT		22		87		60	96	79	100								
Cre02.g122300	GPD5	glycerol-3-P dehydrogenase															
WUSTL-cw15	6	4	6	6	6	8	10	12	11	11	11	14	18	19	18	16	16
WUSTL-sta6	10	6	4	6	7	9	13	17	11	15	12	12	17	18	17	16	14
UCLA1-cw15		4	3	13	11	12	16	19	18								
UCLA1-sta6		4	0	9	13	15	14	12	12								
UCLA-WT		7		7		4	5	7	5								

[a] Green, boost addition; PB, postboost; orange, genes with ≥2-fold increases in expression relative to 48-h NF levels following acetate boost; blue, gene showing strong differential expression between the *sta6* and *cw15* strains.

strongly increase in the *sta6* strain, reaching 217% of their maximum boost levels at 96 h NF (Table 6, blue), such that *GPD3* expression levels at 96 h NF are 12-fold higher in the *sta6* strain than in the *cw15* strain. The distinctive *GPD3* transcription pattern is the fourth of four *sta6*/*cw15* differences that are highlighted this report.

The five *GDP* genes are members of three subfamilies (see Fig. S2 in the supplemental material). The genes in the third subfamily (*GDP2* to *GDP4*) have an additional feature: they carry an N-terminal HAD domain encoding a hydrolase sequence with homology to the enzyme 3-phosphoserine phosphatase (PSP), which catalyzes the final and irreversible step of serine biosynthesis (54). The *Arabidopsis* member of the subfamily lacks this domain, but it is present in the *V. carteri* member. An independent *PSP1* gene in *C. reinhardtii* maintains steady expression throughout 0→96 h NF (not shown). Assuming that the PSP domains of the GPDH proteins are operant, then two enzymatic activities would be stimulated with up-expression of *GPD2-GPD4*.

(v) TCA and glyoxylate cycles. Genes encoding enzymes proposed (8) as components of the tricarboxylic acid (TCA) cycle show either steady or slowly declining 0→48 h NF expression in both strains, with concordant WUSTL and UCLA trajectories (see Table S5A in the supplemental material). Only three genes show upregulation with the boost (see Table S5A, orange). The *CIS2* gene is given further consideration below.

The less familiar glyoxylate cycle, which is absent in animals, shares many enzymes with the TCA cycle and permits the net synthesis of a 4-C product (succinate) from two acetyl units; the succinate is then metabolized to malate/oxaloacetate, which feed into gluconeogenesis. Table S5B in the supplemental material shows the three genes encoding enzymes proposed (8) as components of the glyoxylate cycle that show robust expression, where only *MDH2* shows a modest increase in the *sta6* strain with the acetate boost. Two other genes unique to the glyoxylate cycle, *ICL1* and *MAS1*, show a sensitive expression pattern and a strong stimulation with the boost (see below).

(vi) Acetyl-CoA. Acetate enters both the TCA and glyoxylate cycles as acetyl-CoA, and acetyl-CoA is also the acetate donor for fatty acid biosynthesis. Acetyl-CoA synthetases are encoded by three genes. *ACS1* expression, while steady, is far lower in the *sta6* strain than the *cw15* strain in the WUSTL data but equivalent in the UCLA data (see Table S5C in the supplemental material), again emphasizing the value of having multiple data sets when attempting to discern strain-specific expression patterns. Expression of both *ACS2* and *ACS3* increases with N deprivation in a sensitive fashion, and these genes are discussed below.

A second avenue to acetyl-CoA synthesis is catalyzed by multimeric pyruvate dehydrogenases that convert pyruvate to acetyl-CoA and CO_2. The expression patterns of two genes, *PDH2* (mitochondrial subunit) and *PDC2* (chloroplast subunit) (see Table S5C in the supplemental material), exemplify those encoding the other subunits: transcription is strong and steady to 96 h NF without a boost effect.

A third avenue, the cleavage of citrate via ATP citrate lyase, is important in the generation of acetyl-CoA in the oleaginous yeast *Yarrowia lipolytica* (55), but *ACLA1* and *ACLB1* transcripts are steady during 0⟶96 h NF, and *ACLA1* expression decreases with the boost (see Table S5C in the supplemental material).

Acetyl-CoA can also be generated via acetate kinase (*ACK1* and *ACK2*) and acetylphosphotransferase (*PAT1* and *PAT2*), and while *PAT1* levels are steady, the other three decline >2-fold in expression with the boost (see Table S5C in the supplemental material), suggesting that this pathway is not a major participant.

(vii) Gluconeogenesis/glycolysis and the Calvin-Benson cycle. Gluconeogenesis and the Calvin-Benson cycle both engage in generating hexose phosphates that have two alternative anabolic destinations: feeding into the oxidative pentose phosphate pathway with the concomitant generation of NADPH, or feeding into starch biosynthesis. They can also be catabolized via glycolysis. In a recent review, Johnson and Alric (56) noted that enzymes mediating the "upper half" of gluconeogenesis (from 3-phosphoglycerate to hexose phosphates) appear to be plastid localized in *C. reinhardtii*, where their activities may overlap Calvin-Benson cycle enzyme activities.

The robust members of the gluconeogenesis pathway and Calvin-Benson cycle are listed in Tables S5D and E in the supplemental material, respectively; sensitive members are discussed below. An obvious anomaly is the high initial level of expression of the *RBCS2* gene, encoding the RuBisCO small subunit, in the *sta6* strain compared with the *cw15* strain; however, even higher levels are expressed in the UCLA-WT sample, so the significance of this difference is not clear [the large subunit is chloroplast encoded and not represented in these poly(A)-selected RNA samples]. A few gluconeogenesis/glycolysis genes are mildly up- or downregulated by the boost (see Table S5D in the supplemental material, orange and purple), but overall, expression of both gene sets in both strains is quite steady to 96 h NF except for a decrease in *RBCS2* transcripts and increases in *GAP1* (glyceraldehyde-3-P dehydrogenase), *PYK1* (pyruvate kinase), and *GND1* (6-phosphogluconate dehydrogenase) transcripts.

Fructose-1,6-bisphosphate aldolases (FBA) function in both gluconeogenesis/glycolysis and in the Calvin-Benson cycle. During gluconeogenesis, they catalyze the formation of 6-C fructose-bisphosphate from two 3-C sugars, glyceraldehyde-3-P and dihydroxyacetone phosphate (DHAP), the latter also being the substrate for the glycerol-3-P dehydrogenases mentioned above. The four *FBA* genes in the *C. reinhardtii* genome belong to two subfamilies (see Fig. S3 in the supplemental material). *FBA2* (no predicted leader sequence) and *FBA4* (predicted chloroplast leader), in one subfamily, are expressed at low levels (*FBA4* apparently carries a C-terminal deletion), and only *FBA2* shows a modest (1.7-fold) boost response in the *sta6* strain. *FBA1*, also in this subfamily, and *FBA3*, in the second subfamily, have predicted chloroplast leaders; both show a sensitive expression pattern and a modest upregulation with the boost, as detailed below.

(viii) Pentose phosphate pathway. The oxidative phase of the plastid-localized pentose phosphate pathway takes glucose-6-P to ribulose-5-P, generating 2 NADPHs needed for fatty acid synthesis; the nonoxidative phase generates fructose-6-P and glyceraldehyde-3-P to regenerate the hexose-P that keeps the cycle running. During 0⟶48 h NF, four of the genes encoding enzymes in the pathway—*GND1*, *GLD1*, *GLD2*, and *FSA1*—increase in expression and remain elevated during the next 2 days, while others—*PGL2*, *RPI1*, *TRK1*, and *TAL2*—decrease expression and remain low; *PGL1* transcripts are steady (see Table S5F in the supplemental material). The one gene to display an acetate boost is *TAL1*, encoding transaldolase; it is considered with the other sensitive genes.

Nitrogen-related genes that increase in expression with boost. As expected, and as previously reported (8, 11, 14), N starvation elicits upregulation of numerous genes involved with nitrogen uptake and scavenging. Table S6 in the supplemental material lists the genes encoding N transporters (Table S6A) and enzymes engaged in the transfer of amino groups (Table S6B) whose transcription is stimulated ≥2-fold with acetate boost. Expression patterns are generally concordant between WUSTL and UCLA experiments. Noteworthy are the relatively low levels of expression of *LAO1* and *LAO2*, encoding periplasmic amino acid oxidases, in the *sta6* strain but not the *cw15* strain, the strong and enduring rescue of *PROB1* (glutamate-5-kinase) transcription with the acetate boost in both strains, and the quirky expression patterns of *DUR3A*, a urea transporter. The *AST1* gene, encoding aspartate aminotransferase, is discussed below as a member of the sensitive gene set.

Boyle et al. (8) presented molecular and genetic evidence that the gene *NRR1* encodes a regulator for induction of the TAG accumulation pathway in N-free medium. Supporting this proposal, we found a strong increase in its expression starting at 2 h NF and a 2.3-fold increase with boost in the *sta6* strain (see Table S6C in the supplemental material).

Stress-related genes whose expression increases with the boost. Abrupt N starvation of log-phase cells is by definition stressful. An early response is the stimulated expression of members of the target of rapamycin (TOR)-related autophagy pathway (57). Of the seven annotated *APG* genes (called *ATG* in most organisms) that respond to *TOR* signaling in other organisms, all are strongly and coordinately upregulated starting at 2 h NF, and all except *APG10* remain elevated for the next 96 h, with only *APG4* showing a positive boost response and several showing a modest negative response (see Table S7A in the supplemental material).

Expression of most *PEX*, *PRX*, and *MSD* genes that participate in ROS scavenging remains steady or decreases in both experiments throughout the time course (data not shown), perhaps because chlorophyll levels (8, 9, 13, 25, 48) and photosynthetic electron transport activity (25, 58) decrease and such toxic products are not a major issue. Table S7B in the supplemental material shows the four genes in this category with a modest boost response. None of the genes encoding *SRR* scavenger receptors responds to the boost; *SRR16* shows stronger expression in the *sta6* strain than the *cw15* strain in the WUSTL but not the UCLA data (see Table S7B), yet another example of the value of having 2 data sets.

Table S7C in the supplemental material includes several stress-related low-CO_2-inducible (*LCI*) genes that are boost upregulated and a high-CO_2-inducible (*FEA1*) gene to illustrate that members

of this cohort have highly variable expression patterns both between strains and between experiments.

Respiratory burst oxidase. The gene *RBO1*, encoding a homologue of the respiratory burst oxidase that responds to stress in land plants (59, 60), is contiguous to the *STA6* gene and deleted in the *sta6* mutant (14), suggesting that its absence might influence the *sta6* phenotype (14). As shown in Table S7D in the supplemental material, *RBO1* produces few transcripts in the *cw15* strain and UCLA-WT during 0→48 h NF and is unresponsive to the boost.

A full copy of the contiguous orthologue *RBO2* is present in the *sta6* strain, but it yields few transcripts (see Table S7D in the supplemental material), suggesting that the deletion of *RBO1* curtails *RBO2* expression as well (14). *RBO2* expression is also low in the wild type; in the *cw15* strain, it decreases in the UCLA data and increases in the WUSTL data, where it stabilizes without the boost (see Table S7D).

Blaby et al. (14) noted that in the UCLA experiments, expression of *LHCSR1* and *LHCSR2*, which are both involved in photoquenching, is higher in the *cw15* strain than in the *sta6* strain (see Table S7D in the supplemental material) and suggested that *RBO1*/*RBO2* might play a role in their induction. However, in the WUSTL data, both genes are more strongly transcribed in the *sta6* strain than in the *cw15* strain (see Table S7D).

A key test of this hypothesis—the effect of an *RBO1* transgene on the *sta6* phenotype—is currently in progress in the UCLA labs.

Carbon-related genes with "sensitive" expression patterns.

(i) The blue/green cohort. Five boost-enhanced genes—*ICL1*, *MAS1*, *PCK1*, *TAL1*, and *FBP1*—were of immediate interest because these genes were identified in the UCLA study (14) as having patterns of expression that were similar within a strain but markedly different when the *cw15* and *sta6* strains were compared. Specifically, expression of the five genes sank or stayed low during 0→48 h NF in the *cw15* strain but increased, after an initial drop, in the *sta6* strain (14).

When we analyzed the 0→48 h NF expression patterns of these five genes in the WUSTL data, they also proved to be similar within a strain and distinctive between strains. However, the patterns observed were quite different from those observed in the UCLA study. As shown in Fig. 5, transcription of these genes in the *cw15* strain is high through 12 h NF, drops at 24 h NF, and is <40% of starting values by 48 h NF (blue bars), while transcription in the *sta6* strain generally stays low throughout the time course except for a strong spike at 24 h NF (green bars), when the transcripts are >50% more abundant than at 48 h NF. The RPKM values for these gene sets are presented in Table 7.

We went on to identify 16 additional genes that display the blue/green pattern in the WUSTL data set; all but *ACS2*, *FBA3*, *PGK1*, *PRK1*, and *RPE1* show the late <40% drop in expression (blue) in the *cw15* strain compared with starting values, and all but *CIS2* show the >50% spike in expression (green) in the *sta6* strain at 24 h NF compared with 48 h NF (Fig. 5 and Table 7). Figure S4 in the supplemental material shows WUSTL expression profiles for other genes whose products function in the same pathways as the genes shown in Figure 5, and none displays the blue/green pattern. Most of the 21 genes responded to the acetate boost to at least some extent (Fig. 5); those with a ≥2-fold increase are highlighted in orange in Table 7.

None of the additional 16 genes displays the blue/green pattern in the UCLA1 data, and only *ACS3*, GFY3, and Cre15.g641200 display the *cw15* down/*sta6* up pattern of the five founder UCLA genes (Table 7). Instead, in both UCLA experiments, their expression tends to decrease gradually in both strains (Table 7; also, see Table S8 in the supplemental material). Table S8 also displays data from the UCLA-WT experiment, where expression patterns are again different, with transcript levels generally being higher than those in UCLA-cw.

Unlike the genes grouped together in previous sections, the 21 genes listed in Table 7 encode proteins that operate in a number of different pathways. Isocitrate lyase (*ICL1*) and malate synthase (*MAS1*) are the linchpin enzymes of the glyoxylate cycle; PEP carboxykinase (*PCK1*) and fructose-1,6-bisphosphatase (*FBP1* and *FBP2*), respectively, drive entry into and a late step in gluconeogenesis; acetyl-CoA synthetase (*ACS2* and *ACS3*) feeds acetate into the TCA and glyoxylate cycles and into fatty acid synthesis; candidate acetate permeases (GFY3, GFY4, and GFY5), if verified, would mediate acetate uptake; transaldolase (*TAL1*) and ribulose-phosphate-3-epimerase (*RPE1*) serve in the nonoxidative pentose phosphate pathway; sedoheptulose-1,7-bisphosphatase (*SBP1*) and phosphoribulokinase (*PRK1*) are unique to the Calvin-Benson cycle; Cre15.g641200 is annotated as a candidate mitochondrial fatty acid carrier, although it lacks a mitochondrial targeting sequence; and aspartate aminotransferase (*AST1*) catalyzes the interconversion of aspartate and α-ketoglutarate to glutamate and oxaloacetate, which feeds into the pentose phosphate pathway. The gene products fructose-1,6-bisphosphate aldolase (*FBA1* and *FBA3*), phosphoglycerate kinase (*PGK1*), and glyceraldehyde-6-phosphate dehydrogenase (*GAP3*) are predicted to be members of the Calvin-Benson cycle (14). It should be noted, however, that FBA, PGK, and GAPDH also function in gluconeogenesis, and given that both pathways operate in the chloroplast stroma (56), their activities may not be strictly segregated. An anomaly related to *CIS2* is considered below.

Taken together, it appears that a group of 21 genes, whose products function in various pathways, respond to 0→48 h NF and the acetate boost as a cohort in the WUSTL experiment, whereas their expression patterns differ in both the UCLA and UCLA-WT experiments. We suggest that these differences relate to the fact that the three experiments were performed using different strains (wild type versus mutants) and laboratory conditions (e.g., medium and light intensity; see Materials and Methods) and propose that the listed genes are singularly sensitive to the cell's metabolic status, perhaps because their products serve as "gateway" members of their respective pathways. They might, for example, have short half-lives and/or govern rate-limiting reactions and hence serve as nodes that permit gene expression levels to influence the course of metabolism or biosynthesis. We therefore refer to these as "sensitive genes," as contrasted with the "robust genes," whose expression patterns are concordant, with minor variations, within the three experiments.

Support for this proposal comes from the recent study of an *ICL1* deletion mutant (61), which is devoid of a glyoxylate cycle and displays many anomalies in central carbon metabolism. $^{14}N/^{15}N$ labeling experiments show that many of the proteins designated here as sensitive—specifically, those encoded by *MAS1*, *CIS2*, *FBA1*, *PCK1*, *ACS3*, *TAL1*, and *AST1*—are either strongly increased or decreased in the mutant relative to controls.

(ii) Genes whose expression is stimulated by acetate. Thirteen of the 21 sensitive genes in Table 7 have ≥2-fold increases in expression with the acetate boost (orange highlighting), whereas the others show a weaker or no response. Expression of the

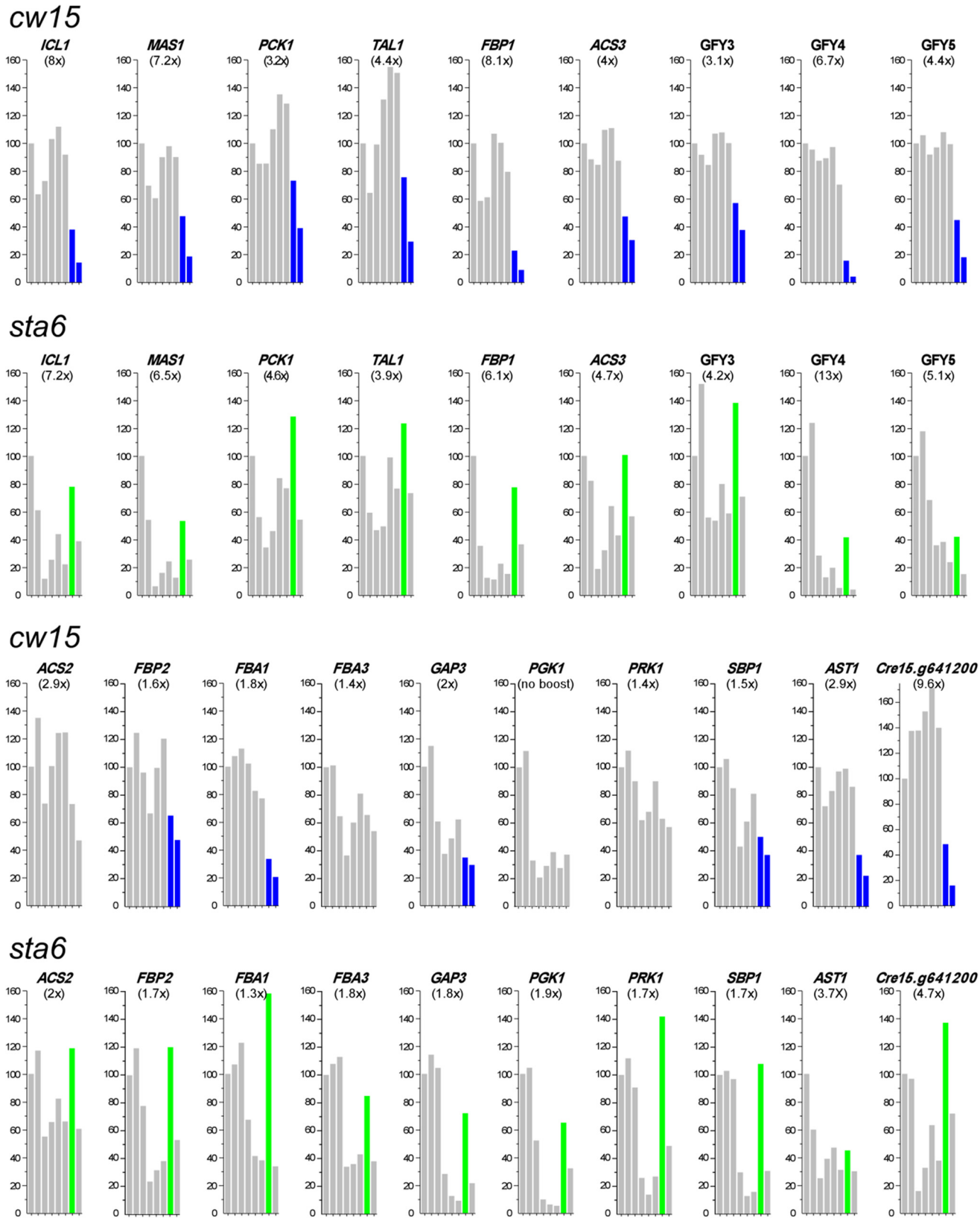

FIG 5 Sensitive gene set. RPKM values at 0 h NF (postcentrifugation) were set at 100; subsequent percentiles are at 0.5, 2, 4, 8, 12, 24, and 48 h NF. RPKM data for these and additional sensitive genes appear in Table 7. A drop in expression in the *cw15* strain occurs at late time points (blue when the 48-h NF value is <40% of the initial value), and a drop in *sta6* expression occurs early, with a spike at 24 h NF (green when the 24-h NF value is at least 50% greater than the 48-h NF value). Numbers in parentheses are fold increases in gene expression in response to the boost (maximum RPKM level during the 2 h postboost divided by RPKM level at 48 h NF).

TABLE 7 Expression profiles (RPKM) of genes showing "sensitive" transcription patterns[a]

	log phase	0 h NF	0.5 h NF	2 h NF	4 h NF	8 h NF	12 h NF	24 h NF	48 h NF	boost	0.5 h PB	2 h PB	4 h PB	8 h PB	12 h PB	24 h PB	48 h PB
SENSITIVE GENES																	
Cre06.g282800	ICL1	isocitrate lyase															
WUSTL-cw15		3077	2407	1525	1755	2482	2697	2212	917	344	472	1458	2752	1508	1089	1042	868	931
WUSTL-sta6		2579	1435	875	169	365	629	317	1118	556	1682	4005	1916	1145	840	723	883	1085
UCLA1-cw15			511	108	141	30	73	97	58	38								
UCLA1-sta6			993	32	28	47	160	287	734	700								
Cre01.g057800	MAS1	malate synthetase																
WUSTL-cw15		1015	851	592	516	767	834	768	405	159	194	396	1134	687	497	466	369	360
WUSTL-sta6		1079	718	388	45	115	174	90	383	183	513	1185	613	460	344	321	320	429
UCLA1-cw15			205	36	57	16	38	47	34	15								
UCLA1-sta6			404	44	13	28	64	102	220	224								
Cre02.g141400	PCK1	PEP carboxykinase																
WUSTL-cw15		1666	1252	1069	1071	1380	1694	1610	917	489	287	663	1585	1260	877	829	636	640
WUSTL-sta6		1352	841	471	288	387	707	646	1079	456	929	1648	2117	1918	1315	1148	1185	1371
UCLA1-cw15			495	142	95	27	44	76	77	80								
UCLA1-sta6			584	136	72	200	310	420	635	599								
Cre01.g032650	TAL1	transaldolase																
WUSTL-cw15		1401	951	612	943	1251	1473	1433	720	280	210	289	1222	900	578	528	427	437
WUSTL-sta6		1159	539	319	251	266	533	413	665	395	613	1430	1553	1107	707	634	655	812
UCLA1-cw15			115	31	110	49	63	92	49	43								
UCLA1-sta6			467	44	110	148	193	308	595	588								
Cre07.g338450	FBP1	fructose bisphosphate phosphatase																
WUSTL-cw15		186	201	118	123	215	202	160	46	18	16	33	148	90	53	52	46	62
WUSTL-sta6		199	178	63	22	20	40	27	138	65	156	400	307	212	131	113	120	169
UCLA1-cw15			106	32	25	16	14	15	8	12								
UCLA1-sta6			96	54	4	6	10	19	66	91								
Cre07.g353450	ACS3	acetyl-CoA synthase																
WUSTL-cw15		1156	978	866	827	1073	1086	856	465	298	355	755	1200	612	477	489	422	437
WUSTL-sta6		1200	709	582	133	228	454	304	715	401	1356	1891	900	569	456	395	504	592
UCLA1-cw15			384	128	155	123	199	216	149	137								
UCLA1-sta6			510	63	116	166	289	326	543	468								
Cre17.g700750	GFY3	candidate acetate permease																
WUSTL-cw15		3080	2509	2303	2121	2688	2706	2514	1433	946	1744	2961	2320	2248	1803	1872	1476	1532
WUSTL-sta6		1748	1032	1567	576	552	825	606	1426	730	2267	3088	1911	1381	1219	1103	1380	1287
UCLA1-cw15			2073	1196	584	543	768	805	600	486								
UCLA1-sta6			1188	524	569	625	922	1116	1665	1277								
Cre17.g702900	GFY4	candidate acetate permease																
WUSTL-cw15		2651	1991	1903	1742	1779	1940	1401	312	84	163	413	561	491	376	334	234	225
WUSTL-sta6		1022	663	821	188	85	130	34	275	26	161	294	337	196	87	76	90	104
UCLA1-cw15			455	375	146	44	61	59	36	19								
UCLA1-sta6			263	66	69	54	75	80	123	77								
Cre17.g702950	GFY5	candidate acetate permease																
WUSTL-cw15		5105	4371	4630	4022	4246	4726	4351	1961	796	1233	2803	3492	2576	2132	1945	1593	1429
WUSTL-sta6		1382	1169	1376	798	418	447	276	490	176	565	893	630	425	294	259	282	298
UCLA1-cw15			1708	2153	1072	623	734	690	411	274								
UCLA1-sta6			731	458	355	291	290	303	338	217								
Cre23.g768500	ACS2	acetyl-CoA synthase																
WUSTL-cw15		308	268	362	197	269	333	334	196	126	151	244	369	239	226	237	210	200
WUSTL-sta6		340	304	355	167	199	250	200	360	184	310	367	314	297	233	233	187	250
UCLA1-cw15			113	214	132	72	105	95	83	68								
UCLA1-sta6			136	92	141	209	177	165	166	114								
Cre12.g510650	FBP2	fructose bisphosphate phosphatase																
WUSTL-cw15		224	262	327	252	175	261	316	171	125	206	165	182	234	270	238	190	187
WUSTL-sta6		306	258	308	201	61	82	99	310	138	123	147	165	159	142	142	114	108
UCLA1-cw15			316	603	363	244	129	160	234	218								
UCLA1-sta6			221	261	286	129	115	157	192	103								
Cre01.g006950	FBA1	fructose bisphosphate aldolase																
WUSTL-cw15		88	92	99	104	94	76	71	31	19	35	21	26	30	32	31	27	28
WUSTL-sta6		191	161	172	197	175	106	61	254	54	48	40	68	68	52	56	38	48
UCLA1-cw15			98	156	118	57	28	24	29	24								
UCLA1-sta6			107	103	173	188	100	97	62	30								
Cre05.g234550	FBA3	fructose bisphosphate aldolase																
WUSTL-cw15		1941	2313	2344	1499	846	1394	1875	1520	1252	1625	1285	1711	1945	2070	1991	1638	1642
WUSTL-sta6		3432	3258	3520	3684	1112	1174	1415	2765	1249	1279	1321	2302	1916	1636	1752	1731	1575
UCLA1-cw15			1952	3083	1200	726	419	627	1173	1297								
UCLA1-sta6			1932	2122	3800	1629	727	1229	1499	947								
Cre01.g010900	GAP3	glyceraldehyde-6-P dehydrogenase																
WUSTL-cw15		1385	1747	2007	1058	652	856	1084	606	513	1026	481	622	790	887	900	736	676
WUSTL-sta6		2930	2771	3155	2890	778	340	246	1989	594	638	556	1050	763	642	706	531	547
UCLA1-cw15			2112	3158	1078	627	212	245	497	651								
UCLA1-sta6			2005	2318	3150	1039	352	565	728	373								
Cre22.g763250	PGK1	phosphoglycerate kinase																
WUSTL-cw15		392	476	532	157	99	139	186	132	177	182	90	161	185	196	211	198	191
WUSTL-sta6		813	655	684	341	64	40	34	427	210	176	119	396	316	258	266	272	279
UCLA1-cw15			478	832	162	52	6	6	22	73								
UCLA1-sta6			470	443	332	79	24	60	106	92								
Cre12.g554800	PRK1	phosphoribulokinase																
WUSTL-cw15		585	667	744	599	414	452	603	417	380	514	280	418	530	602	596	474	467
WUSTL-sta6		892	733	820	663	188	156	207	1038	361	347	350	612	496	471	495	399	384
UCLA1-cw15			644	987	633	258	93	133	269	324								
UCLA1-sta6			511	483	663	295	208	359	428	248								
Cre03.g185550	SBP1	sedoheptulose-1,7-bisphosphatase																
WUSTL-cw15		581	663	706	564	287	405	536	332	223	364	229	338	441	527	491	353	348
WUSTL-sta6		1056	927	956	902	274	122	147	1001	287	285	347	480	380	334	360	268	270
UCLA1-cw15			880	1186	714	202	123	182	357	387								
UCLA1-sta6			649	637	979	524	164	282	403	200								
Cre12.g511900	RPE1	ribulose phosphate-3-epimerase																
WUSTL-cw15		193	222	298	222	222	473	614	493	453	649	409	536	743	856	777	626	600
WUSTL-sta6		228	194	236	110	36	65	142	805	310	307	285	289	351	405	437	241	263
UCLA1-cw15			160	241	78	66	48	67	79	77								
UCLA1-sta6			169	183	58	30	36	58	72	48								
Cre15.g641200		candidate mitochondrial fatty acid carrier																
WUSTL-cw15		550	320	440	411	489	548	448	155	51	57	169	496	256	179	167	129	143
WUSTL-sta6		497	228	220	36	74	144	86	312	163	514	760	428	278	218	171	199	251
UCLA1-cw15			100	19	30	5	15	20	13	9								
UCLA1-sta6			159	5	6	9	39	70	231	198								
Cre02.g122250	AST1	aspartate aminotransferase																
WUSTL-cw15		444	362	262	301	351	359	312	135	80	90	184	231	155	109	109	84	90
WUSTL-sta6		355	299	179	76	117	140	94	134	89	180	328	218	164	130	107	111	150
UCLA1-cw15			129	28	67	59	64	60	42	38								
UCLA1-sta6			235	84	29	58	76	77	121	115								
Cre03.g149100	CIS2	citrate synthase																
WUSTL-cw15		840	636	597	519	589	609	507	270	188	152	285	462	294	221	223	207	218
WUSTL-sta6		544	461	330	102	155	257	204	189	121	310	416	349	262	211	178	209	251
UCLA1-cw15			244	52	98	89	119	134	97	103								
UCLA1-sta6			347	71	56	103	160	155	185	174								

[a] Light green, boost addition; PB, postboost; blue, drop in *cw15* transcripts at 24 h NF and 48 h NF; dark green, increase in *sta6* transcripts at 24 h NF; orange, genes with ≥2-fold increases in expression relative to 48 h NF levels following the acetate boost.

strongly boost-responsive set is also highly sensitive to the presence of exogenous acetate in N-replete medium. Table 8 compares their transcript levels during N-replete log-phase growth in acetate-containing medium (WUSTL) versus acetate-free medium (UTSW) (26). The genes that show ≥2-fold responses to the acetate boost prove to be expressed at very low levels when the strain is grown on acetate-free medium (Table 8A, columns 3 and 4) compared with acetate-containing medium (Table 8A, columns 1, 2, and 7), with low expression persisting after 18 h NF in acetate-free medium (Table 8A, columns 5 and 6). In contrast, sensitive genes showing modest or no boost responses are expressed equivalently (Table 8B) or at higher levels (Table 8C) when the strains are grown on acetate-free medium compared with acetate-containing medium, with expression usually declining after 18 h NF in acetate-free medium. Hence sensitive genes displaying a strong acetate boost prove to also display a strong transcriptional sensitivity to the presence/absence of exogenous acetate. Notably, 7 of these 13 proteins, listed in the previous paragraph, are also expressed aberrantly in the *ICL1* mutant (61).

In the course of this analysis, we encountered an anomaly pertaining to the *CIS1* and *CIS2* (citrate synthase) genes. The former has been predicted to encode a glyoxylate cycle enzyme and the latter to encode a TCA cycle enzyme (14), assignments that have been adopted in Table S5A and B in the supplemental material. However, *CIS2* shows a strong acetate boost upregulation and low expression on acetate-free medium (Table 8A), akin to the dedicated *ICL1* and *MAS1* enzymes of the glyoxylate cycle (Table 8A), whereas *CIS1* is non-boost-responsive (see Table S5A), like other TCA cycle genes (Table S5A), and equivalently expressed in both media (Table 8B). Plancke et al. (61) also presented arguments for *CIS2* as a member of the glyoxylate cycle.

A second anomaly relates to the glyoxylate cycle itself. Both the UCLA1 and UCLA2 studies document increased levels of expression of *ICL1*, *MAS1*, and *CIS2* in the *sta6* strain and low expression levels in the *cw15* strain and complemented *sta6* strains during 0⟶48 h NF and suggest that enhanced glyoxylate activity plays a role in enhanced TAG production in the *sta6* strain. However, this increase is not observed in the WUSTL data. Miller et al. (11), who also observed decreases in *ICL1* and *MAS1* expression in wild-type N-starved cells, pointed out that depressed glyoxylate cycle activity would result in more acetate being available for fatty acid biosynthesis. The phenotype of the *ICL1* deletion mutant (57) supports their proposal: the mutant generates enhanced levels of fatty acids and TAGs compared with non-deletion-containing controls even under N-replete conditions. It has also been reported that hexose phosphates, which accumulate in the *sta6* strain (14), inhibit expression of *ICL* and *MAS* genes in cucumber (62). Taken together, the enhanced *sta6* glyoxylate cycle profiles in the UCLA studies during 0⟶48 h NF, confirmed with enzyme assays, presumably reflect particular features of the UCLA experimental conditions and may explain, at least in part, why TAG levels in the *sta6* strain were found to be equivalent to those in the *cw15* strain at 48 h NF and were not enhanced until 96 h NF, whereas they were enhanced by 48 h NF under WUSTL experimental conditions (18, 24).

Figure 6 shows (in blue) the products of the 13 acetate-sensitive genes and their positions in various metabolic/biosynthetic pathways. We propose that of the 21 blue/green genes identified in this study (Tables 7 and 8), this cluster monitors a variety of activities related to acetate utilization, while the remaining 8 genes largely monitor activities related to the Calvin-Benson cycle.

(iii) Candidate acetate permeases. The genes designated GFY3, GFY4, and GFY5 in Tables 7 and 8, as well as the genes GFY1 and GFY2, have been identified as members of the *GPR1*/

TABLE 8 Expression profiles (RPKM) of genes listed in Table 7 in the presence or absence of acetate[a]

Acetate		+	+	-	-	-	-	+	
Growth phase		log	log	log	log	18 h NF	18 h NF	0 h NF	≥ 2x increase with boost
Synchrony		asynch	asynch	asynch	synch	synch mt+	synch mt-	asynch.	
Strain		*cw15*	*sta6*	wt	wt	wt	wt	wt	
Source		WUSTL	WUSTL	UTSW	UTSW	UTSW	UTSW	UCLA	
ACETATE-SENSITIVE GENES									
(A) Low expression in - acetate media									
Cre06.g282800	ICL1	3077	2579	17	77	0	0	2271	+
Cre01.g057800	MAS1	1015	1079	2	3	1	8	557	+
Cre02.g141400	PCK1	1666	1352	9	11	12	8	707	+
Cre01.g032650	TAL1	1401	1159	63	212	77	34	263	+
Cre07.g338450	FBP1	186	199	10	112	0	0	134	+
Cre07.g353450	ACS3	1156	1200	33	54	20	15	562	+
Cre23.g768500	ACS2	308	340	16	15	12	7	133	+
Cre03.g149100	CIS2	840	544	33	77	51	43	338	+
Cre17.g700750	GFY3	3080	1748	47	51	6	9	3557	+
Cre17.g702900	GFY4	2651	1022	2	0	0	0	1311	+
Cre17.g702950	GFY5	5105	1382	6	4	0	6	5961	+
Cre15.g641200		550	497	11	50	0	0	114	+
Cre02.g122250	AST1	444	355	16	44	34	27	153	+
(B) Equivalent expression in +N, +/- acetate media									
Cre05.g234550	FBA3	1941	3432	3802	5235	814	613	4019	-
Cre01.g010900	GAP3	1385	2930	3857	5994	298	101	5198	-
Cre22.g763250	PGK1	392	831	486	789	6	9	628	-
Cre12.g554800	PRK1	585	892	931	995	140	57	1078	-
Cre03.g185550	SBP1	581	1056	1548	1994	244	72	1596	-
Cre12.g514750	CIS1	58	78	40	23	92	81	40	-
(C) Enhanced expression in +N, - acetate media									
Cre12.g510650	FBP2	224	306	679	681	251	141	397	-
Cre12.g511900	RPE1	193	228	612	432	377	337	323	-
Cre01.g006950	FBA1	88	191	258	359	42	18	349	-

[a] All genes with low expression without exogenous acetate have ≥2-fold increases in expression with acetate boost (Table 7).

FUN30/*YaaH* (pfam01184) gene family (63) (see Fig. S4A in the supplemental material). Several fungal proteins encoded by genes in this family have been shown or suggested to mediate acetate uptake (64, 65), and acetate permease activity has recently been demonstrated for the *E. coli* protein YaaH (66). In *S. cerevisiae*, both exogenous acetate and induction of the glyoxylate cycle are accompanied by strong upregulation of its *GPR1*/*FUN30*/*YaaH* gene (67, 68).

In *C. reinhardtii*, the five genes are closely linked on LG17, with GFY1 to GFY3 in one cluster and GFY4 and GFY5 apparently contiguous in a second cluster.

While GFY1 and GFY2 show constitutive expression and GFY1 transcripts actually decrease with the boost, GFY3 to GFY5 show the blue/green pattern during 0→48 h NF (Fig. 5) and an increase in expression of 3- to 13-fold with the acetate boost in both strains (Fig. 5 and Table 7). Expression of GFY3 to GFY5 is also strong in the UCLA and UCLA-WT samples (Table 7), all of which derive from cells maintained in acetate, whereas cells grown or maintained in the absence of acetate have very low reads (Table 8A).

We went on to analyze this family in more detail using two approaches. Figure S5B in the supplemental material shows a similarity network (38, 39) of 355 representative *GPR1*/*FUN30*/*YaaH* sequences (a key is provided in Data Set S6 in the supplemental material). The proteins are widely disseminated and clearly separate along the eukaryote/prokaryote divide, with members absent from animals and vascular land plants. The genomes of sequenced algal species encode orthologs (see Data Set S6) that bear greater similarity to the prokaryotic proteins than the other eukaryotic proteins (see Fig. S5B), suggesting that the nonalgal eukaryotes (mostly fungi) and algae independently acquired the genes from prokaryotes by horizontal gene transfer (HGT) in two distinct and early events. Maximum-likelihood analysis (Fig. S5C) shows that the green-algal genes form a loose clade, clade III, that is again more closely related to prokaryotic (clade I) than to eukaryotic (clade II) family members, and Fig. S5D in the supplemental material shows that the six genes in *V. carteri* form a subfamily distinct from the five genes in the closely related *C. reinhardtii*, highlighting the rapid evolution of these sequences in algal lineages. The phylogenetic distributions of *GPR1*/*FUN30*/*YaaH* genes can be highly unusual, with both moss and fungal genes being found in clade II, a *Leishmania* gene being found in the prokaryotic clade I (presumably a recent HGT), and volvocacean genes being more closely related to a haptophyte gene (*E. huxleyi*) than to other chlorophyte genes in clade III.

Schönknecht et al. (69) independently performed a phylogenetic analysis of this gene family and published a topology wherein eukaryotic algal and fungal/moss proteins share a direct common ancestry and together form a clade that is sister to the prokaryotic members. Subsequent analyses using their data (kindly provided by G. Schönknecht) revealed that the topology of the two major eukaryotic clusters is highly sensitive to evolutionary models and parameters used for phylogenetic reconstruction and can yield

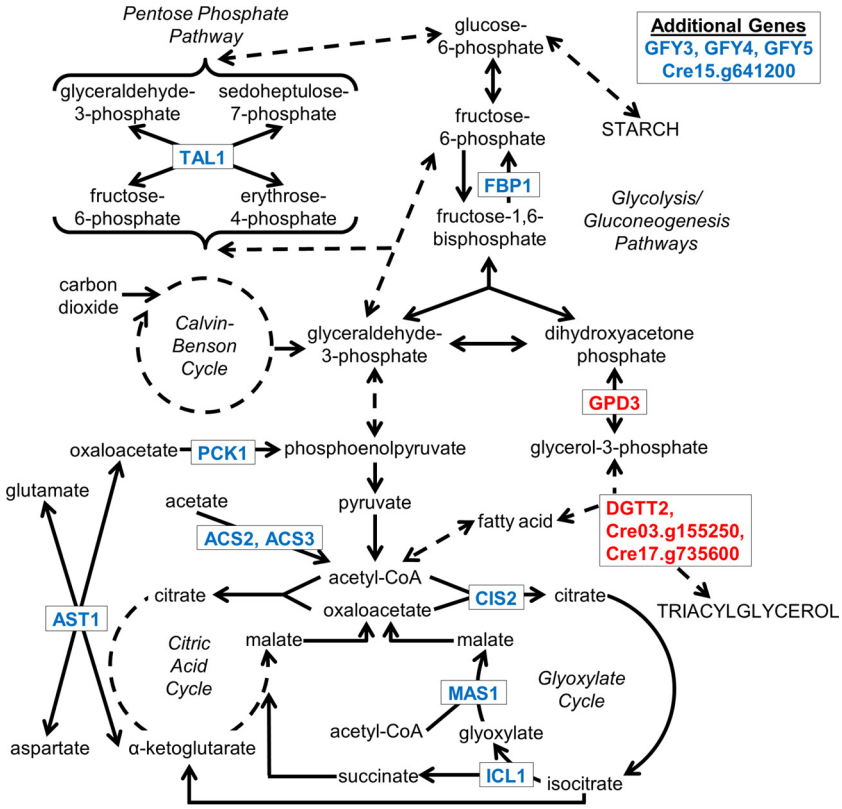

FIG 6 Proteins encoded by the acetate-sensitive gene set (blue font) and by genes selectively upregulated in the *sta6* strain (red font). Abbreviations: ACS, acetyl-CoA synthetase; AST, aspartate transaminase; CIS, citrate synthase; Cre03.g155250 and Cre17.g735600, candidate TAG synthase enzymes; Cre15.g641200, candidate mitochondrial fatty acid carrier; DGTT, diacylglycerol acyltransferase type 2; FBP, fructose-1,6-bisphosphatase; GFY, GPR1/FUN30/YaaH family (candidate acetate transporters); GPD, glycerol phosphate dehydrogenase; ICL, isocitrate lyase; MAS, malate synthase; PCK, phosphoenolpyruvate carboxykinase; TAL, transaldolase.

well-supported trees in either of two configurations: green algae and fungi/moss as separate HGT events from bacteria, as depicted in Fig. S5C in the supplemental material, or green algae (but not *Galdieria*) and fungi/moss as a single HGT event, as depicted in reference 69.

Our network analysis of the *GPR1/FUN30/YaaH* family (see Fig. S5B in the supplemental material) supports the tree topology in Fig. S5C in clearly distinguishing the fungal/moss members and the green-algal members as separate offshoots of the central prokaryotic cluster. In both of our analyses, the unusual phylogenetic relationships among the eukaryotic members of the family, noted above, suggest that subsequent HGT took place between disparate eukaryotic groups.

Stress-related genes that decrease in expression with the boost. Whereas only a few stress-related genes are upregulated with the acetate boost (see Table S7 in the supplemental material), a far larger group of stress-related genes is down-regulated ≥2-fold with the boost, with the low point usually occurring at 30 min postboost (Table 9, purple). More genes are so affected in the *sta6* strain (64 genes) than in the *cw15* strain (40 genes); in Table 9, those not downregulated in the *cw15* strain are italicized. The downregulated genes, some of which have been identified in a recent study of autophagy in *C. reinhardtii* (73), encode proteasome subunits, chaperones, heat shock proteins, and proteins that participate in degradative processes, the one apparent outlier being *BCS1*, which encodes a mitochondrial biogenesis factor. We went on to identify 20 additional nonannotated genes that also show this pattern in both strains (Table 9, purple); these may prove to be members of the same response cohort.

Of the 41 non-proteasome-encoding genes in Table 9, 22 share an additional pattern: their expression increases 2- to 6-fold (means of 3.3-fold ± 0.9-fold for the *cw15* strain and 3.5-fold ± 1.4-fold for the *sta6* strain) between the 24-h NF sample (see Table S9 in the supplemental material, blue) and the 48-h NF sample (see Table S9, yellow), followed by the sharp boost-induced decrease lifted up in Table 9 (see Table S9, purple). The 11 genes in red in Table 9 show this blue/yellow/purple pattern in both strains (see Table S9A); the 11 in blue show the pattern in the *sta6* strain only (see Table S9B). The 20 nonannotated genes in Table 9 also show the blue/yellow/purple pattern (see Table S9C), except for the 5 italicized entries, where it is seen only in the *sta6* strain, again suggesting that these genes are members of the same cohort as the annotated set. While not invariably the case, the genes in the *sta6* strain usually show a larger increase at 48 h NF than the genes in the *cw15* strain.

In the UCLA experiments, where the boost was not performed, none of the 22 annotated genes shows increased expression at 48 h NF in the *cw15* strain (see Table S9A in the supplemental material). However, 12 of the 22 show a modest (mean of 2.1-fold ± 0.4-fold) increase in the *sta6* strain (see Table S9A and B in the supplemental material), as do 8 of the 20 nonannotated genes (data not shown).

TABLE 9 Expression profiles (RPKM) of *sta6* genes whose expression decreases ≥2-fold relative to 48 h NF levels following acetate boost (purple)[a]

			48 h NF	boost	0.5 h PB	2 h PB
DEGRADATIVE						
Proteasomes						
Cre01.g011500	RPN11	26S proteasome regulatory subunit	75	75	31	38
Cre01.g030850	POA4	20S proteasome α subunit D	43	37	12	22
Cre01.g066650	RPN1	26S proteasome regulatory subunit	44	41	16	21
Cre06.g275650	RPN3	26S proteasome regulatory subunit	35	26	11	20
Cre06.g279000	PBA1	20S proteasome β subunit A1	51	44	25	35
Cre06.g280850	PBG1	20S proteasome β subunit, type 4	52	45	25	36
Cre06.g304300	POA6	20S proteasome α subunit F	57	53	23	29
Cre07.g329700	RPT2	26S proteasome regulatory subunit	115	100	44	55
Cre08.g373250	POA2	20S proteasome α subunit B	56	46	18	34
Cre10.g418100	POA3	20S proteasome α subunit C	59	54	21	31
Cre10.g424400	PBB1	20S proteasome β subunit B, type β2	74	59	28	37
Cre10.g461950	PBE1	20S proteasome β subunit E, type β5	49	41	18	30
Cre13.g581450	RPN7	26S proteasome regulatory subunit	43	34	16	21
Cre13.g601100	RPN8	26S proteasome regulatory subunit	54	44	12	21
Cre14.g619550	POA7	20S proteasome α subunit G	75	56	25	37
Cre14.g625400	RPT1	26S proteasome regulatory subunit	74	62	20	32
Cre16.g663500	RPN10	26S proteasome regulatory subunit	28	28	9	15
Cre14.g610950	PBD1	20S proteasome β subunit D, type 2	96	89	31	49
Cre17.g705400	POA1	20S proteasome α subunit A	69	66	28	45
Cre17.g708300	RPN12	26S proteasome regulatory subunit	49	43	19	26
Cre17.g710150	RPT4	26S proteasome regulatory subunit	61	52	22	32
Cre17.g724350	POA5	20S proteasome α subunit E	61	55	15	28
Cre17.g727950	RPN2	26S proteasome regulatory subunit	31	30	11	13
Heat-shock proteins and other chaperones						
Cre02.g080650	HSP90B	heat shock protein 90B	305	167	64	135
Cre02.g080700	BIP1	heat shock protein 70, ER	242	159	69	123
Cre10.g439900	HSP70G	ER-located HSP110/SSE-like protein	88	61	10	30
Cre14.g617400	HSP22F	heat shock protein 22F	441	259	41	51
Cre14.g617450	HSP22E	heat shock protein 22E	335	248	81	69
Cre01.g060000	HSP22C	heat shock protein 22C	12	5	6	6
Cre02.g090850	CLPB3	ClpB chaperone, Hsp100 family	105	71	26	33
Cre03.g189950	HOP1	HSP70-HSP90 organizing protein	52	26	11	27
Cre06.g309100	CPN60C	chaperonin 60C, HSP60 homologue	115	70	20	84
Cre09.g386750	HSP90A	heat shock protein 90A	687	368	163	288
Cre18.g746450	CLPB1	ClpB chaperone, Hsp100 family	54	13	12	24
Cre07.g341550	p23	p23 co-chaperone of HSP90 system	81	62	30	76
Cre08.g372100	HSP70A	heat shock protein 70A	599	214	198	212
Cre09.g393200	HSP70C	heat shock protein 70C	99	72	19	76
Cre16.g677000	HSP70E	heat shock protein 70E	97	74	37	69
Cre17.g707950	HEP2	Hsp70 escorting protein 2	28	22	14	16
Other degradative						
Cre04.g224800	VAMP74	R-SNARE protein, VAMP72-family	160	14	6	12
Cre11.g468050	VIPP2	vesicle inducing plastid protein	44	27	6	12
Cre12.g498500	DEG11/ DEG1C	DegP-type protease	112	66	20	19
Cre17.g725750		mis-folded RNA adaptor	95	45	4	11
Cre17.g726850		mis-folded RNA adaptor	121	28	9	20
Cre24.g768900	BCS1	ubiquinol:cytochrome c oxidoreductase biogenesis factor	105	31	5	7
Cre02.g135150	FKB62	peptidyl-prolyl *cis-trans* isomerase	61	28	11	21
Cre03.g179100		ubiquitin fusion degradation protein	16	6	3	4
Cre06.g281350	LON1	mitochondrial LON protease	19	14	8	10
Cre10.g429001		E2-ubiquitin conjugating enzyme	15	17	7	5
Cre10.g447800		mis-folded RNA adaptor	77	58	21	31
Cre01.g047700	CYN40	peptidyl-prolyl cis-trans isomerase	17	11	8	9
Cre01.g066450	SUMO97	small ubiquitin-like modifier	12	9	3	7
Cre01.g070050	DCL2	dicer-like protein	17	11	5	7
Cre02.g088400	DEG1A	DegP-type protease	19	13	9	14
Cre03.g152750		BAG domain protein	17	1	1	3
Cre06.g267700	SPP1B	signal peptide peptidase	17	15	4	8
Cre08.g382689	UBQ3	bi-ubiquitin	9	6	4	5
Cre09.g386400	UBA1	ubiquitin-activating enzyme E1	130	100	41	86
Cre12.g483550	VPE1	vacuolar processing enzyme	27	21	12	14
Cre12.g526700	RBL9	rhomboid-like protease	37	25	7	14
Cre13.g583550	VIPP1	vesicle inducing plastid protein	267	206	98	126
Cre16.g664800	RBL4	rhomboid-like protease	22	14	11	14
Cre18.g746300	RBL3	rhomboid-like protease	15	8	5	6
Cre26.g772100	VMS1	VCP/Cdc48-associated mitochondrial stress responsive 1	14	8	6	7
Non-annotated						
Cre01.g015500			42	9	10	11
Cre02.g095200			60	35	5	14
Cre02.g098800			36	17	8	12
Cre03.g149250			111	79	9	20
Cre06.g283900			73	29	18	13
Cre06.g298850			60	22	6	10
Cre07.g348350			57	23	10	10
Cre07.g355850			139	79	53	33
Cre09.g413150			48	13	8	9
Cre10.g435200			52	19	13	18
Cre12.g505050			109	50	6	16
Cre12.g510500			53	23	15	19
Cre12.g513600			53	18	11	23
Cre12.g551100			84	27	12	25
Cre12.g554400			361	113	15	53
Cre13.g580000			784	322	26	35
Cre14.g619250			226	86	77	46
Cre16.g676600			75	39	5	13
Cre17.g697400			83	19	17	14
Cre17.g723750			159	92	27	32

[a] Genes that do not show this pattern in the *cw15* strain are shown in italics. The genes in colored type also show an increase in expression at 48 h NF relative to 24 h NF (see Table S7 in the supplemental material): red indicates that the pattern is present in *cw15* and *sta6* strains, and blue indicates that it is present in the *sta6* strain only. PB, postboost.

As detailed in the Discussion, we propose that this increase/decrease pattern in degradation-related genes may relate to our morphological observation (Fig. 2 and 3) that an acetate boost at 48 h NF appears to divert cells from pursuing an autophagocytic pathway.

DISCUSSION

General overview of the TAG-accumulation response. This study, combined with those previously published, generates the following picture of the TAG accumulation response, which, while provisional and incomplete, can serve to provide context for a discussion of our results.

C. reinhardtii cells growing in acetate-supplemented N-replete medium actively run acetate-fed glyoxylate cycles and photosynthetic electron transport-fed Calvin-Benson cycles. When the cells are transferred into N-free acetate medium, these cycles presumably continue to operate in the short term, generating glucose-6-P via both the Calvin-Benson cycle and the glyoxylate cycle-derived oxaloacetate, which feeds into gluconeogenesis.

Early in the first day, genes encoding starch-related enzymes are upregulated, and much of the glucose-6-P is funneled into ADP-glucose and then starch biosynthesis in the *cw15* strain but not in the *sta6* strain. During the first day, genes encoding enzymes for glycerol-3-P, fatty acid, and TAG biosynthesis are also upregulated in specific patterns, while genes encoding enzymes for the glyoxylate cycle are in most cases downregulated, presumably allowing exogenous acetate to funnel into fatty acid biosynthesis. TAGs proceed to accumulate in cytoplasmic LBs (in both strains) and in chloroplast LBs (in the *sta6* strain but not the *cw15* strain).

By the end of the second day, when starch levels start to plateau (9, 17, 48), the cells ordinarily shift into an autophagy program that limits the extent of TAG accumulation, possibly because its execution is dependent on TAG breakdown. If, however, they are subjected to an acetate boost, this program is bypassed, for unknown reasons, and the cells instead continue to accumulate TAG until, in the *sta6* strain, they reach full obesity. Along the way, chlorophyll levels and rates of photosynthetic electron transport diminish, meaning that cells are increasingly reliant on glucose-6-P entry into the pentose phosphate pathway to generate the NADPH needed for fatty acid synthesis. Key participants in these various transitions are 21 "sensitive" genes whose transcription levels, we suggest, are responsive to the overall operation of various metabolic pathways, with 13 being responsive to the cells' acetate status.

Given this context, we first discuss what has been learned about the differences between starch-forming strains, in particular the *cw15* strain, and the starchless *sta6* mutant. We then discuss what has been learned about the role of the acetate boost in long-term TAG accumulation.

Comparisons of the *cw15* and *sta6* strains. The original premise of this study was that the *cw15* strain was the parent of the *sta6* strain, but the careful work of Blaby et al. (14) has established that this is not the case, leading them to focus much of their inquiry on comparing the *sta6* mutant with complemented *sta6* strains. However, the responses to N-free conditions in the *cw15* strain and in complemented *sta6* strains proved to be generally similar (14).

A major observation of the study by Blaby et al. (14), supported by assays of enzyme activity and metabolite profiles, is that *sta6*

cells increase expression of five key genes—*ICL1*, *MAS1*, *PCK1*, *TAL1*, and *FBP1*—during 0→48 h NF, whereas expression of these genes in starch-forming strains is low during this period, suggesting that the glyoxylate and gluconeogenesis pathways are more active in the *sta6* strain than in starch-producing strains. In the WUSTL study, wherein different media and light conditions were used (see Materials and Methods), these five genes also share common patterns of expression, but the shared patterns are different from the UCLA patterns: in the *cw15* strain, transcripts remain elevated until 24 h NF and then drop to lower levels, while in the *sta6* strain, transcript levels are low except for a curious and unexplained spike in abundance at 24 h NF which abates by 48 h NF. We went on to identify 16 additional genes in the WUSTL data set whose patterns of expression match those of the first five, where most of these 21 genes also respond to acetate boost (Fig. 5 and Table 7). Several of the genes in this cohort are also anomalously expressed in a mutant strain that has a deletion of the isocitrate lyase gene (*ICL1*) and hence is blocked in its glyoxylate cycle (61). We suggest that the transcription patterns of this "sensitive" gene set are indicative of the biochemical pathways being pursued by cells under a given set of environmental/genetic conditions and that they may be less informative in indicating the defining differences between starch-forming and starch-null cells.

With the important caveat that half the *C. reinhardtii* genes have not yet been annotated, and some of these may play key roles in storage product biology, four genes, in red in Fig. 6, have been identified whose expression is markedly distinctive between the *sta6* and starch-forming strains under various laboratory conditions: *DGTT2*, encoding one of several diacylglycerol acyltransferases (first noted in reference 14); Cre03.g155250 and Cre17.g735600, encoding candidate lipases; and *GPD3*, encoding one of five glycerol-3-P dehydrogenases.

DGTT2 and the candidate lipases are strongly overexpressed in the *sta6* strain compared with starch-forming strains even in N-replete medium (Tables 4 and 5). While it is straightforward to posit correlations between enhanced DGTT2 levels and TAG accumulation, it is counterintuitive to posit such correlations for lipases. However, the recent work of Li et al. (50) documents that a gene annotated as encoding a TAG lipase, and now called *PDG1*, in fact participates in TAG biosynthesis under N-free conditions, and Cre03.g155250 is a homologue of *PDG*. A full characterization of the Cre03.g155250 and Cre17.g735600 gene products and gene knockdowns is clearly highly warranted.

Glycerol-3-P dehydrogenases (GPDHs) catalyze the formation of glycerol-3-P, the backbone of lipid molecules, from dihydroxyacetone phosphate (DHAP), which is, in turn, formed by the cleavage of fructose bisphosphate via fructose bisphosphate aldolase (FBA). Aldolases associate with both gluconeogenesis and the Calvin-Benson cycle, and two of the four FBA-encoding genes in *C. reinhardtii* are members of the sensitive gene cohort (Table 7).

The *C. reinhardtii* genome encodes five GPDH enzymes. Of these, GPDH2 and GPDH4 are predicted to be chloroplastic, and expression of their corresponding genes increases steadily during 48 h→N, with *GPD4* transcripts generally being 1.5- to 2-fold higher in the *sta6* strain than in the *cw15* strain (Table 6). The *GPD3* gene, with no predicted targeting sequence, is poorly expressed in all tested strains during 0→48 h NF. However, with the acetate boost, its transcription is strongly enhanced, far more so in the *sta6* strain than in the *cw15* strain, to 96 h NF (Table 6). Little attention has been given to a possible role for glycerol-3-P levels in influencing rates of DAG/TAG biosynthesis (19, 22), but these profiles suggest that an exploration of this possibility could be fruitful.

While these four gene expression differences between the *cw15* and *sta6* strains may well prove to participate in generating the *sta6* phenotype, the phenotype is also likely to be influenced at the metabolic level by what we can term a glucose-6-P backflow. Blaby et al. (14) showed that levels of glucose-6-P are 2-fold higher in the *sta6* strain at 96 h NF than in complemented starch-forming strains, similar to two starch-null mutants of *Arabidopsis* that accumulate hexose monomers (70, 71). Moreover, the WUSTL and UCLA data both indicate that *sta6* cells are fully committed to forming starch, expressing the relevant enzymes at the same levels and for the same time periods as do starch-forming cells (Table 2). Hence glucose-6-P is presumably generated and sent to the starch-biosynthetic apparatus in a normal fashion. When, in the *sta6* strain, it fails to be converted into glucose-ADP and undergo polymerization, it presumably has to go somewhere, the obvious possibility being that it is somehow involved in the formation of chloroplast LBs (18).

The widely accepted model for LB formation in land plants is that fatty acids are synthesized in the chloroplast and then shuttled to the ER, where they are conjugated to glycerol-3-P backbones by resident ER enzymes to generate DAGs and then TAGs. Recent studies, however, indicate that TAG biosynthesis in *C. reinhardtii* has a number of distinctive features (summarized in Fig. 9 of reference 50): (i) the DAG moieties are largely assembled in the plastid, and some are then shipped to the ER for the addition of a third acyl group (16); (ii) many of the TAG fatty acids derive from pre-existing chloroplast glycerolipids that are cleaved by dedicated lipases such as PDG1 (50); and (iii) the closely apposed chloroplast outer envelope membrane and ER membranes (18) are coparticipants in cytoplasmic LB assembly, perhaps assisted by alga-specific and ER-localized MLDP proteins (12, 49). Another relevant consideration is that *C. reinhardtii* likely possesses at least one chloroplast-localized diacylglycerol acyltransferase that mediates the constitutive formation of TAG-filled plastoglobules and eyespot granules in all strains (12, 18).

One *sta6* scenario, then, would go as follows. (i) Some of the posited glucose-6-P backflow feeds into the plastid-localized pentose phosphate pathway to generate the NADPH required for additional fatty acid synthesis as photosynthetic electron transfer abates. (ii) Some of the backflow moves in the glycolysis direction until it forms fructose bisphosphate, some of which is then shunted into glycerol-3-P via enhanced levels of GPDH enzymes, where the sharply reduced level of fructose bisphosphate in N-starved *sta6* cells (14) is consistent with this suggestion. (iii) The backflow may also inhibit operation of the glyoxylate cycle, as is observed in land plants (62), directing acetate into fatty acid biosynthesis. (iv) The augmented fatty acid and glycerol-3-P pools, supplemented by the products of thylakoid breakdown (18), generate augmented levels of chloroplast DAG, some of which is then converted into chloroplast TAG, events mediated by the enhanced levels of DGTT2 and Cre03.g155250/Cre17.g735600 enzymes. (v) The TAG is stored in chloroplast-localized LBs, perhaps via an expansion of pre-existing plastoglobules (18). Testable features of this model include the prediction that mutations in the four *sta6*-enhanced enzymes would compromise chloroplast LB formation in a *sta6* background and that these enzymes are chloroplast localized.

Mutations like the *sta6* deletion are expected to generate a loss-of-function phenotype, in this case an inability to form starch. Unexpected is a gain-of-function phenotype, in this case the formation of a novel class of LBs with the attendant upregulation of at least four lipid-related genes. Chloroplast LBs have a well-defined organization and architecture (18), which is also unexpected for a cellular trait generated by a biochemical defect. Hence, it is possible that the *sta6* genotype elicits the expression of a chloroplast-LB biosynthetic program, encoded in the *C. reinhardtii* genome, which is not called upon in wild-type cells under normal laboratory conditions but is stimulated in wild-type cells under to-be-identified conditions.

Acetate boost. The acetate boost was discovered by accident: an additional 20 mM acetate was inadvertently added to a culture at 48 h NF, and we noticed that the cells went on to accumulate far larger LBs than nonboosted cells. In our earlier study (18), the effects of the boost were monitored by light and electron microscopy, where both cytoplasmic and chloroplast LB size was more strongly enhanced in the *sta6* strain than in the *cw15* strain.

We document here that the rate of acetate depletion from medium boosted to 40 mM acetate is unchanged from the rate of depletion at 20 mM acetate (Fig. 4), countering hypotheses that the boosted cells simply take up additional acetate for fatty acid and hence TAG biosynthesis.

That said, there apparently occurs at least a pulse of acetate entry when the boost is administered, as documented by two events: (i) 229 flagellum-related genes are transiently upregulated in expression in the *cw15* strain, the classic response to the acetic acid-mediated "pH shock" used to deflagellate *C. reinhardtii* cells (43); and (ii) ~1,300 additional genes are either up- or downregulated in expression ≥2-fold following boost in both strains (Table 1), with most quickly returning to preboost levels. Only a few of the upregulated genes encode enzymes in pathways for starch or lipid biosynthesis (Tables 2 to 5), but many encode proteins involved in nitrogen uptake and scavenging (see Table S6 in the supplemental material) and in pathways of central carbon metabolism (Tables 6 and 7; also, see Table S5 in the supplemental material).

Of particular interest are 13 strongly boost-upregulated genes whose expression is low when cells are grown or N starved in medium lacking exogenous acetate (Table 8 and Fig. 6, blue font), suggesting that these genes carry upstream regulatory elements responsive to the cell's acetate status. Interestingly, a different set of genes, involved with spore formation, is coordinately upregulated by acetate in *S. cerevisiae* (68).

Hence, assuming that these transcripts are translated, one consequence of the boost is to endow cells with enhanced levels of key transporters and enzymes for the ensuing days of N starvation and TAG formation.

Two observations form the basis for an additional hypothesis on the influence of the boost. By microscopy, we noticed that starting at 48 h NF, nonboosted cells come to contain large cytoplasmic vacuoles (Fig. 2), filled with degrading cellular material (Fig. 3), a response that does not occur in boosted cells. The nonboosted cells are fully viable (see Table S1 in the supplemental material), indicating that this autophagy program is a "natural" and not a toxic response to N deprivation, but it is accompanied by a smaller accumulation of TAG in nonboosted cells.

We then noticed, in analyzing the 875 *sta6* genes whose transcription is downregulated by the acetate boost, a set of 64 genes encoding proteins that are expected to participate in protein quality control and autophagocytic processes, including proteasome subunits, chaperones, heat shock proteins, cyclophilins, and proteases (Table 9). Moreover, 22 of these genes show a sharp increase in expression in the *sta6* strain during the day immediately prior to the boost (see Table S9 in the supplemental material), where an additional 20 nonannotated genes also show this pattern as well and may represent additional members of the cohort. Hence, expression of a sizable autophagy-related gene subset is either simply downregulated by the boost or else first stimulated at 48 h NF and the stimulation then aborted by boost. In both sets of experiments, the *cw15* strain is less responsive to the proposed "autophagy signal" than is the *sta6* strain, possibly because it is less stressed due to its starch reserves. These data suggest that the boost is able, for unknown reasons, to signal to the *sta6* strain that it is not necessary to pursue the autophagy program, thereby enabling the cells to follow the path to full obesity.

ACKNOWLEDGMENTS

We thank Bill Snell (UT Southwestern) for helpful discussions of his RNA-Seq results.

This work was supported by contract DE-EE0003046 (to U.G., S.J., S.S.M., and M.P.) via the National Alliance for Advanced Biofuels and Bioproducts (NAABB) from the U.S. Department of Energy (DOE) and by Cooperative Agreement DE-FC02-02ER63421 from the DOE Office of Science (BER) to the Institute of Genomics and Proteomics, UCLA. Support to U.G. from grant DE-SC0006873 from the DOE Office of Science (BER), to J.-H.L. from grant 2013M1A8A1056300 from the Korea CCS R&D Center (KCRC), Korean Ministry of Science, to I.B. from training grant T32 ES015457 from the National Institutes of Health, and to S.D.G. and S.S.M. from grant R24 GM092473 from the National Institutes of Health is acknowledged.

REFERENCES

1. **Liu B, Benning C.** 2013. Lipid metabolism in microalgae distinguishes itself. Curr. Opin. Biotechnol. **24:**300–309. http://dx.doi.org/10.1016/j.copbio.2012.08.008.
2. **Merchant SS, Kropat J, Liu B, Shaw J, Warakanont J.** 2012. TAG, you're it! Chlamydomonas as a reference organism for understanding algal triacylglycerol accumulation. Curr. Opin. Biotechnol. **23:**352–363. http://dx.doi.org/10.1016/j.copbio.2011.12.001.
3. **Hu Q, Sommerfeld M, Jarvis E, Ghirardi M, Posewitz M, Seibert M, Darzins A.** 2008. Microalgal triacylglycerols as feedstocks for biofuel production: perspectives and advances. Plant J. **54:**621–639. http://dx.doi.org/10.1111/j.1365-313X.2008.03492.x.
4. **Rodolfi L, Chini Zittelli G, Bassi N, Padovani G, Biondi N, Bonini G, Tredici MR.** 2009. Microalgae for oil: strain selection, induction of lipid synthesis and outdoor mass cultivation in a low-cost photobioreactor. Biotechnol. Bioeng. **102:**100–112. http://dx.doi.org/10.1002/bit.22033.
5. **Wijffels RH, Kruse O, Hellingwerf KJ.** 2013. Potential of industrial biotechnology with cyanobacteria and eukaryotic microalgae. Curr. Opin. Biotechnol. **24:**405–413. http://dx.doi.org/10.1016/j.copbio.2013.04.004.
6. **Harris EH.** 2009. The Chlamydomonas sourcebook. I. Introduction to Chlamydomonas and its laboratory use. Elsevier, Amsterdam, The Netherlands.
7. **Merchant SS, et al.** 2007. The Chlamydomonas genome reveals the evolution of key animal and plant functions. Science **318:**245–250. http://dx.doi.org/10.1126/science.1143609.
8. **Boyle NR, Page MD, Liu B, Blaby IK, Casero D, Kropat J, Cokus S, Hong-Hermesdorf A, Shaw J, Karpowicz SJ, Gallaher S, Johnson S, Benning C, Pellegrini M, Grossman A, Merchant SS.** 2012. Three acyltransferases and a nitrogen responsive regulator are implicated in nitrogen starvation-induced triacylglycerol accumulation in *Chlamydomonas*. J. Biol. Chem. **287:**15811–15825. http://dx.doi.org/10.1074/jbc.M111.334052.
9. **Cakmak T, Angun P, Demiray YE, Ozkan AD, Elibol Z, Tekinay T.** 2012. Differential effects of nitrogen and sulfur deprivation on growth and

biodiesel feedstock production of *Chlamydomonas reinhardtii*. Biotechnol. Bioeng. **109:**1947–1957. http://dx.doi.org/10.1002/bit.24474.
10. **James GO, Hocart CH, Hillier W, Chen H, Kordbacheh F, Price GD, Djuordjevic MA.** 2011. Fatty acid profiling of *Chlamydomonas reinhardtii* under nitrogen deprivation. Bioresour. Technol. **102:**3343–3351. http://dx.doi.org/10.1016/j.biortech.2010.11.051.
11. **Miller R, Wu G, Deshpande RR, Vieler A, Gärtner K, Li X, Moellering ER, Zäuner S, Cornish AJ, Liu B, Bullard B, Sears BB, Kuo M-H, Hegg EL, Shachar-Hill Y, Shiu S-H, Benning C.** 2010. Changes in transcript abundance in *Chlamydomonas reinhardtii* following nitrogen deprivation predict diversion of metabolism. Plant Physiol. **154:**1737–1752. http://dx.doi.org/10.1104/pp.110.165159.
12. **Moellering ER, Benning C.** 2010. RNA interference silencing of a major lipid droplet protein affecting lipid droplet size in *Chlamydomonas reinhardtii*. Eukaryot. Cell **9:**97–106. http://dx.doi.org/10.1128/EC.00203-09.
13. **Msanne J, Xu D, Konda AR, Casas-Mollano JA, Awada T, Cahoon EB, Cerutti H.** 2012. Metabolic and gene expression changes triggered by nitrogen deprivation in the photoautotrophically grown microalgae *Chlamydomonas reinhardtii* and *Coccomyxa* sp. C-169. Phytochemistry **75:**50–59. http://dx.doi.org/10.1016/j.phytochem.2011.12.007.
14. **Blaby IK, Glaesener AG, Mettler T, Fitz-Gibbon ST, Gallaher SD, Liu B, Boyle NR, Kropat J, Stitt M, Johnson S, Benning C, Pellegrini M, Casero D, Merchant SS.** 2013. Systems-level analysis of nitrogen starvation-induced modifications of carbon metabolism in a *Chlamydomonas reinhardtii* starchless mutant. Plant Cell **25:**4305–4323. http://dx.doi.org/10.1105/tpc.113.117580.
15. **Zabawinski C, Van Den Koornhuyse N, D'Hulst C, Schlichting R, Giersch C, Delrue B, Lacroix J-M, Preiss J, Ball S.** 2001. Starchless mutants of *Chlamydomonas reinhardtii* lack the small subunit of a heterotetrameric ADP-glucose pyrophosphorylase. J. Bacteriol. **183:**1069–1077. http://dx.doi.org/10.1128/JB.183.3.1069-1077.2001.
16. **Fan J, Andre C, Xu C.** 2011. A chloroplast pathway for the de novo biosynthesis of triacylglycerol in *Chlamydomonas reinhardtii*. FEBS Lett. **585:**1985–1991. http://dx.doi.org/10.1016/j.febslet.2011.05.018.
17. **Fan J, Yan C, Andre C, Shanklin J, Schwender J, Xu C.** 2012. Oil accumulation is controlled by carbon precursor supply for fatty acid synthesis in *Chlamydomonas reinhardtii*. Plant Cell Physiol. **53:**1380–1390. http://dx.doi.org/10.1093/pcp/pcs082.
18. **Goodson C, Roth R, Wang ZT, Goodenough U.** 2011. Structural correlates of cytoplasmic and chloroplast lipid body synthesis in *Chlamydomonas reinhardtii* and stimulation of lipid body production with acetate boost. Eukaryot. Cell **10:**1592–1606. http://dx.doi.org/10.1128/EC.05242-11.
19. **Lee YJ, Jeschke GR, Roelants FM, Thorner J, Turk BE.** 2012. Reciprocal phosphorylation of yeast glycerol-3-phosphate dehydrogenases in adaptation to distinct types of stress. Mol. Cell. Biol. **32:**4705–4717. http://dx.doi.org/10.1128/MCB.00897-12.
20. **Li H, Chiu C.** 2010. Protein transport into chloroplasts. Annu. Rev. Plant Biol. **61:**157–180. http://dx.doi.org/10.1146/annurev-arplant-042809-112222.
21. **Ramanan R, Kim B-H, Cho D-H, KoS-R, Oh H-M, Kim H-S.** 2013. Lipid droplet synthesis is limited by acetate availability in starchless mutant of *Chlamydomonas reinhardtii*. FEBS Lett. **587:**370–377. http://dx.doi.org/10.1074/jbc.M109.097758.
22. **Shen W, Li JQ, Dauk M, Huang Y, Periappuram C, Wei Y, Zou J.** 2010. Metabolic and transcriptional responses of glycerolipid pathways to a perturbation of glycerol 3-phosphate metabolism in *Arabidopsis*. J. Biol. Chem. **285:**22957–22965. http://dx.doi.org/10.1074/jbc.M109.097758.
23. **Velmurugan N, Sung M, Yim SS, Park MS, Yang JW, Jeong KJ.** 2013. Evaluation of intracellular lipid bodies in *Chlamydomonas reinhardtii* strains by flow cytometry. Bioresour. Technol. **138:**30–37. http://dx.doi.org/10.1016/j.biortech.2013.03.078.
24. **Wang ZT, Ullrich N, Joo S, Waffenschmidt S, Goodenough U.** 2009. Algal lipid bodies: stress induction, purification, and biochemical characterization in wild-type and starchless *Chlamydomonas reinhardtii*. Eukaryot. Cell **8:**1856–1868. http://dx.doi.org/10.1128/EC.00272-09.
25. **Work VH, Radakovits R, Jinkerson RE, Meuser JE, Elliott LG, Vinyard DJ, Laurens LML, Dismukes GC, Posewitz MC.** 2010. Increased lipid accumulation in the *Chlamydomonas reinhardtii sta7-10* starchless isoamylase mutant and increased carbohydrate synthesis in complemented strains. Eukaryot. Cell **9:**1251–1261. http://dx.doi.org/10.1128/EC.00075-10.
26. **Ning J, Otto TD, Pfander C, Schwach F, Brochet M, Bushell E, Goulding D, Sanders M, Lefebvre PA, Pei J, Grishin NV, Vanderlaan G, Billker O, Snell WJ.** 2013. Comparative genomics in *Chlamydomonas* and *Plasmodium* identifies an ancient nuclear envelope protein family essential for sexual reproduction in protists, fungi, plants, and vertebrates. Genes Dev. **27:**1198–1215. http://dx.doi.org/10.1101/gad.212746.112.
27. **Yoon K, Han D, Li Y, Sommerfeld M, Hu Q.** 2012. Phospholipid: diacylglycerol acyltransferase is a multifunctional enzyme involved in membrane lipid turnover and degradation while synthesizing triacylglycerol in the unicellular green microalga *Chlamydomonas reinhardtii*. Plant Cell **24:**3708–3724. http://dx.doi.org/10.1105/tpc.112.100701.
28. **Sueoka N.** 1960. Mitotic replication of deoxyribonucleic acid in *Chlamydomonas reinhardi* [sic]. Proc. Natl. Acad. Sci. U. S. A. **46:**83–91. http://dx.doi.org/10.1073/pnas.46.1.83.
29. **Gorman DS, Levine RP.** 1965. Cytochrome *f* and plastocyanin: their sequence in the photosynthetic electron transport chain of *Chlamydomonas reinhardtii*. Proc. Natl. Acad. Sci. U. S. A. **54:**1665–1669. http://dx.doi.org/10.1073/pnas.54.6.1665.
30. **Hutner SH, Provasoli L, Schatz A, Haskins CP.** 1950. Some approaches to the study of the role of metals in the metabolism of microorganisms. Proc. Am. Philos. Soc. **94:**152–170.
31. **Kropat J, Hong-Hermesdorf A, Casero D, Ent P, Castruita M, Pellegrini M, Merchant SS, Malasarn D.** 2011. A revised mineral nutrient supplement increases biomass and growth rate in *Chlamydomonas reinhardtii*. Plant J. **66:**770–780. http://dx.doi.org/10.1111/j.1365-313X.2011.04537.x.
32. **Tardif M, Atteia A, Specht M, Cogne G, Rolland N, Brugière S, Hippler M, Ferro M, Bruley C, Peltier G, Vallon O, Cournac L.** 2012. Predalgo: a new subcellular localization prediction tool dedicated to green algae. Mol. Biol. Evol. **29:**3625–3639. http://dx.doi.org/10.1093/molbev/mss178.
33. **Huelsenbeck JP, Ronquist F.** 2001. MRBAYES: Bayesian inference of phylogenetic trees. Bioinformatics **17:**754–755. http://dx.doi.org/10.1093/bioinformatics/17.8.754.
34. **Edgar RC.** 2004. MUSCLE: a multiple sequence alignment method with reduced time and space complexity. BMC Bioinformatics **5:**113. http://dx.doi.org/10.1186/1471-2105-5-113.
35. **Tamura K, Peterson D, Peterson N, Stecher G, Nei M, Kumar S.** 2011. MEGA5: molecular evolutionary genetics analysis using maximum likelihood, evolutionary distance, and maximum parsimony methods. Mol. Biol. Evol. **28:**2731–2739. http://dx.doi.org/10.1093/molbev/msr121.
36. **Guindon S, Dufayard J-F, Lefort V, Anisimova M, Hordijk W, Gascuel O.** 2010. New algorithms and methods to estimate maximum-likelihood phylogenies: assessing the performance of PhyML 3.0. Syst. Biol. **59:**307–321. http://dx.doi.org/10.1093/sysbio/syq010.
37. **Abascal F, Zardoya R, Posada D.** 2005. ProtTest: selection of best-fit models of protein evolution. Bioinformatics **21:**2104–2105. http://dx.doi.org/10.1093/bioinformatics/bti263.
38. **Atkinson HJ, Morris JH, Ferrin TE, Babbitt PC.** 2009. Using sequence similarity networks for visualization of relationships across diverse protein superfamilies. PLoS One **4:**e4345. http://dx.doi.org/10.1371/journal.pone.0004345.
39. **Blaby-Haas CE, Merchant SS.** 2012. The ins and outs of algal metal transport. Biochim. Biophys. Acta **1823:**1531–1552. http://dx.doi.org/10.1016/j.bbamcr.2012.04.010.
40. **UniProt Consortium.** 2011. Ongoing and future developments at the Universal Protein Resource. Nucleic Acids Res. **39:**D214–D219. http://dx.doi.org/10.1093/nar/gkq1020.
41. **Smoot ME, Ono K, Ruscheinski J, Wang PL, Ideker T.** 2011. Cytoscape 2.8: new features for data integration and network visualization. Bioinformatics **27:**431–432. http://dx.doi.org/10.1093/bioinformatics/btq675.
42. **Wittkop T, Emig D, Truss A, Albrecht M, Böcker S, Baumbach J.** 2011. Comprehensive cluster analysis with transitivity clustering. Nat. Protoc. **6:**285–295. http://dx.doi.org/10.1038/nprot.2010.197.
43. **Albee AJ, Kwan AL, Lin H, Granas D, Stormo GD, Dutcher SK.** 2013. Identification of cilia genes that affect cell-cycle progression using whole-genome transcriptome analysis in *Chlamydomonas reinhardtii*. G3 **3:**979–991. http://dx.doi.org/10.1534/g3.113.006338.
44. **Cheshire JL, Evans JH, Keller LR.** 1994. Ca^{2+} signaling in the *Chlamydomonas* flagellar regeneration system: cellular and molecular responses. J. Cell Sci. **107:**2491–2498.
45. **Hartzell LB, Hartzell HC, Quarmby LM.** 1993. Mechanisms of flagellar excision. I. The role of intracellular acidification. Exp. Cell Res. **208:**148–153.
46. **Augstein A, Barth K, Gentsch M, Kohlwein SD, Barth G.** 2003. Characterization, localization and functional analysis of Bpr1p, a protein affecting sensitivity to acetic acid in the yeast *Yarrowia lipolytica*. Microbiology **149:**589–600. http://dx.doi.org/10.1099/mic.0.25917-0.

47. **Gentsch M, Barth G.** 2005. Carbon source dependent phosphorylation of the Gpr1 protein in the yeast *Yarrowia lipolytica*. FEMS Yeast Res. **5:**909–917. http://dx.doi.org/10.1016/j.femsyr.2005.04.009.
48. **Siaut M, Cuiné S, Cagnon C, Fessler B, Nguyen M, Carrier P, Beyly A, Beisson F, Triantaphylidès C, Li-Beisson Y, Peltier G.** 2011. Oil accumulation in the model green alga *Chlamydomonas reinhardtii*: characterization, variability between common laboratory strains and relationship with starch reserves. BMC Biotechnol. **11:**7. http://dx.doi.org/10.1186/1472-6750-11-7.
49. **Huang NL, Huang MD, Chen TL, Huang AH.** 2013. Oleosin of subcellular lipid droplets evolved in green algae. Plant Physiol. **161:**1862–1874. http://dx.doi.org/10.1104/pp.112.212514.
50. **Li X, Moellering ER, Liu B, Johnny C, Fedewa M, Sears BB, Kuo MH, Benning C.** 2012. A galactoglycerolipid lipase is required for triacylglycerol accumulation and survival following nitrogen deprivation in *Chlamydomonas reinhardtii*. Plant Cell **24:**4670–4686. http://dx.doi.org/10.1105/tpc.112.105106.
51. **Ham HJ, Rho HJ, Shin SK, Yoon H-J.** 2010. The *TGL2* gene of *Saccharomyces cerevisiae* encodes and active acylglycerol lipase located in the mitochondria. J. Biol. Chem. **285:**3005–3013. http://dx.doi.org/10.1074/jbc.M109.046946.
52. **Villarejo, A., Buren, S. Larsson, S. Dejardin, A. Monne, M. Rudhe, C. Karlsson, J. Jansson, S. Lerouge, P. Rolland, N. et al.** 2005. Evidence for a protein transported through the secretory pathway en route to the higher plant chloroplast. Nat. Cell Biol. **7:**1224–1231. http://dx.doi.org/10.1038/ncb1330.
53. **Larsson C, Pahlman I, Ansell R, Rigoulet M, Adler L, Gustafsson L.** 1998. The importance of the glycerol 3-phosphate shuttle during aerobic growth of *Saccharomyces cerevisiae*. Yeast **14:**347–357. http://dx.doi.org/10.1002/(SICI)1097-0061(19980315)14:4<347::AID-YEA226>3.0.CO;2-9.
54. **Jung T-Y, Kim Y-S, Oh B-H, Woo E.** 2013. Identification of a novel ligand binding site in phosphoserine phosphatase from the hyperthermophilic archaeon *Thermococcus onnumineus*. Proteins **81:**819–829. http://dx.doi.org/10.1002/prot.24238.
55. **Beopoulos A, Chardot T, Nicaud J-M.** 2009. *Yarrowia lipolytica*: A model and a tool to understand the mechanisms implicated in lipid accumulation. Biochimie **91:**692–696. http://dx.doi.org/10.1016/j.biochi.2009.02.004.
56. **Johnson X, Alric J.** 2013. Central carbon metabolism and electron transport in *Chlamydomonas reinhardtii*: metabolic constraints for carbon partitioning between oil and starch. Eukaryot. Cell **12:**776–793. http://dx.doi.org/10.1128/EC.00318-12.
57. **Pérez-Pérez ME, Florencio FJ, Crespo JL.** 2010. Inhibition of target of rapamycin signaling and stress activate autophagy in *Chlamydomonas reinhardtii*. Plant Physiol. **152:**1874–1888. http://dx.doi.org/10.1104/pp.109.152520.
58. **Li Y, Han D, Hu G, Dauvillee D, Sommerfeld M, Ball S, Hu Q.** 2010. *Chlamydomonas* starchless mutant defective in ADP glucose pyrophosphorylase hyper-accumulates triacylglycerol. Metab. Eng. **12:**387–391. http://dx.doi.org/10.1016/j.ymben.2010.02.002.
59. **Marino D, Dunand C, Puppo A, Pauly N.** 2012. A burst of plant NADPH oxidases. Trends Plant Sci. **17:**9–15. http://dx.doi.org/10.1016/j.tplants.2011.10.001.
60. **Suzuki N, Miller G, Morales J, Shulaev V, Torres MA, Mittler R.** 2011. Respiratory burst oxidases: the engines of ROS signaling. Curr. Opin. Plant Biol. **14:**691–699. http://dx.doi.org/10.1016/j.pbi.2011.07.014.
61. **Plancke C, Vigeolas H, Höhner R, Roberty S, Emonds-Alt B, Larosa V, Willamme F, Duby F, Onga Dhali D, Thonart P, Hiligsmann S, Franck F, Eppe G, Cardol P, Hippler M, Remacle C.** 2014. Lack of isocitrate lyase in *Chlamydomonas* leads to changes in carbon metabolism and in the response to oxidative stress under mixotrophic growth. Plant J. **77:**404–417. http://dx.doi.org/10.1111/tpj.12392.
62. **Graham IA, Denby KJ, Leaver CJ.** 1994. Carbon catabolite repression regulates glyoxylate cycle gene expression in cucumber. Plant Cell **6:**761–772. http://dx.doi.org/10.1105/tpc.6.5.761.
63. **Casal M, Paiva S, Queirós O, Soares-Silva I.** 2008. Transport of carboxylic acids in yeast. FEMS Microbiol. Rev. **32:**974–994. http://dx.doi.org/10.1111/j.1574-6976.2008.00128.x.
64. **Gentsch M, Kuschel M, Schlegel S, Barth G.** 2007. Mutations at different sites in members of the Fpr1/Fun34/YaaH protein family cause hypersensitivity to acetic acid in *Saccharomyces cerevisiae* as well as in *Yarrowia lipolytica*. FEMS Yeast Res. **7:**380–390. http://dx.doi.org/10.1111/j.1567-1364.2006.00191.x.
65. **Paiva S, Devaux F, Barbosa S, Jacq C, Casal M.** 2004. Ady2P is essential for the acetate permease activity in the yeast *Saccharomyces cerevisiae*. Yeast **21:**201–210. http://dx.doi.org/10.1002/yea.1056.
66. **Sá-Pessoa J, Paiva S, Ribas D, Silva IJ, Viegas SC, Arraiano CM, Casal M.** 2013. SATP (YaaH), a succinate-acetate transporter protein in *Escherichia coli*. Biochem. J. **454:**585–595. http://dx.doi.org/10.1042/BJ20130412.
67. **Lorenz MC, Fink GR.** 2001. The glyoxylate cycle is required for fungal virulence. Nature **412:**83–86. http://dx.doi.org/10.1038/35083594.
68. **Taxis C, Keller P, Kavagiou Z, Juhl Jensen L, Colombelli J, Bork P, Stelzer EHK, Knop M.** 2005. Spore number control and breeding in *Saccharomyces cerevisiae*: a key role for a self-organizing system. J. Cell Biol. **171:**627–640. http://dx.doi.org/10.1083/jcb.200507168.
69. **Schönknecht G, Chen W-H, Ternes CM, Barbier GG, Shrestha RP, Stanke M, Bräutigam A, Baker BJ, Banfield JF, Garavito RM, Carr K, Wilkerson C, Rensing SS, Gagneul D, Dicenson NE, Oesterhelt C, Lercher MJ, Weber APM.** 2013. Gene transfer from bacteria and archaea facilitated evolution of an extremophilic eukaryote. Science **339:**1207–1210. http://dx.doi.org/10.1126/science.1231707.
70. **Caspar T, Huber SC, Somerville C.** 1985. Alterations in growth, photosynthesis, and respiration in a starchless mutant of *Arabidopsis thaliana* (L.) deficient in chloroplast phosphoglucomutase activity. Plant Physiol. **79:**11–17. http://dx.doi.org/10.1104/pp.79.1.11.
71. **Ragel P, Streb S, Feil R, Sahrawy M, Grazia Annunziata M, Lunn JE, Zeeman S, Mérida Á.** 2013. Loss of starch granule initiation has a deleterious effect on the growth of Arabidopsis plants due to an accumulation of ADP-glucose. Plant Physiol. **163:**75–85. http://dx.doi.org/10.1104/pp.113.223420.
72. **Li Y, Ham D, Hu G, Sommerfeld M, Hu Q.** 2010. Inhibition of starch synthesis results in overproduction of lipids in *Chlamydomonas reinhardtii*. Biotechnol. Bioeng. **107:**258–268. http://dx.doi.org/10.1002/bit.22807.
73. **Ramundo S, Casero D, Mühlhaus T, Hemme D, Sommer F, Crèvecoeur M, Rahire M, Schroda M, Rusch J, Goodenough U, Pellegrini M, Perez-Perez ME, Crespo JL, Merchant S, Schaad O, Civic N, Rochaix JD.** Conditional depletion of the chloroplast ClpP1 protein activates nuclear genes involved in autophagy and plastid protein quality control. Plant Cell, in press.